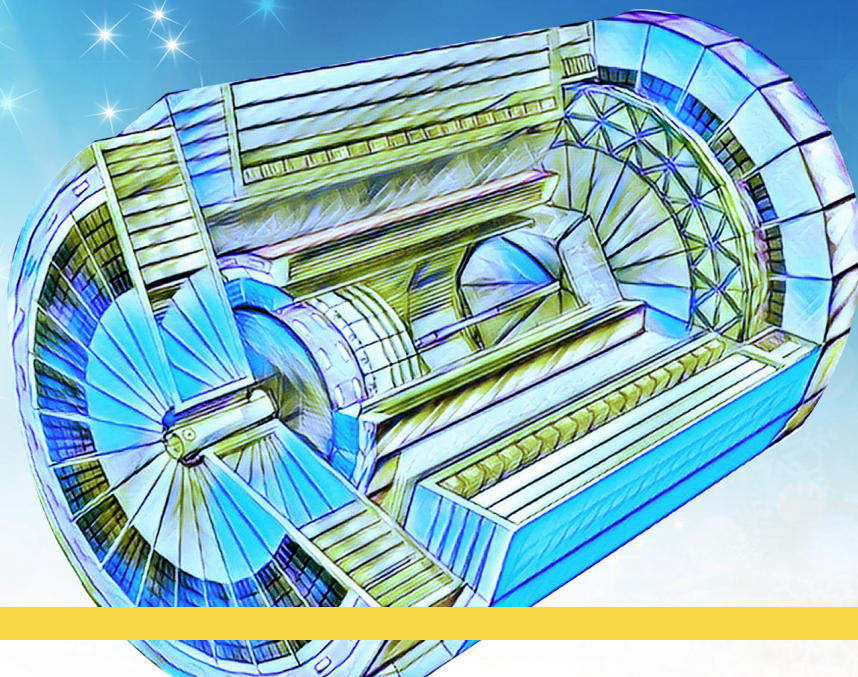




# SCIENCE REQUIREMENTS AND DETECTOR CONCEPTS FOR THE ELECTRON-ION COLLIDER

EIC Yellow Report



Executive Summary

Cover Art by Yulia Furletova and Shannon West

# **Science Requirements and Detector Concepts for the Electron-Ion Collider**

EIC Yellow Report Executive Summary

**full document available online:**

<https://arxiv.org/abs/2103.05419>

April 2021



## Preface

The document summarizes the physics case, the resulting detector requirements, and the evolving detector concepts for the experimental program at the Electron-Ion Collider (EIC) as found in the EIC Yellow Report. The EIC will be a powerful new high-luminosity facility in the United States with the capability to collide high-energy electron beams with high-energy proton and ion beams, providing access to those regions in the nucleon and nuclei where their structure is dominated by gluons. Moreover, polarized beams in the EIC will give unprecedented access to the spatial and spin structure of the proton, neutron, and light ions. The studies leading to this document were commissioned and organized by the EIC User Group with the objective of advancing the state and detail of the physics program and developing detector concepts that meet the emerging requirements in preparation for the realization of the EIC. The effort aims to provide the basis for further development of concepts for experimental equipment best suited for the science needs, including the importance of two complementary detectors and interaction regions.



# Contents

Title Page	i
Preface	iii
Table of Contents	1
1 The Electron-Ion Collider	3
2 Physics Measurements and Requirements	6
3 Detector Concepts	23
4 Opportunities for Detector Technology and Computing	30
Appendix A Deep Inelastic Scattering Kinematics	35
Appendix B Author List	43
Appendix C Organizational Structure	47
Appendix D Acknowledgements	49
References	53





# Chapter 1

## The Electron-Ion Collider

The Electron-Ion Collider (EIC) is a new, innovative, large-scale particle accelerator facility conceived by U.S. nuclear and accelerator physicists over two decades and planned for construction at Brookhaven National Laboratory on Long Island, New York by the U.S. Department of Energy in the 2020s. The EIC will study protons, neutrons and atomic nuclei with the most powerful electron microscope, in terms of versatility, resolving power and intensity, ever built. The resolution and intensity is achieved by colliding high-energy electrons with high-energy protons or (a range of different) ion beams. The EIC provides the capability of colliding beams of polarized electrons with polarized beams of light ions, and this all at high intensity. The EIC was established as the highest priority for new construction in the 2015 US Nuclear Physics Long Range Plan, and was favorably endorsed by a committee established by the National Academy of Sciences in 2018 to assess the science case. In December 2019, the EIC was granted Critical Decision Zero (CD0) by the US Department of Energy, which launched the EIC as an official project of the US government.

The main design requirements of the EIC are:

- Highly polarized electron ( $\sim 70\%$ ) and proton ( $\sim 70\%$ ) beams
- Ion beams from deuterons to heavy nuclei such as gold, lead, or uranium
- Variable  $e+p$  center-of-mass energies from 20–100 GeV, upgradable to 140 GeV
- High collision electron-nucleon luminosity  $10^{33} - 10^{34} \text{ cm}^{-2} \text{ s}^{-1}$
- Possibility to have more than one interaction region

Several of the above performance parameters will be realized for the first time at EIC in a collider mode, such as the availability of nuclear beams and polarized nucleon beams along with the operation at high collision luminosity. Shown schematically in Fig. 1.1, the EIC will collide bright, intense counter circulating beams of

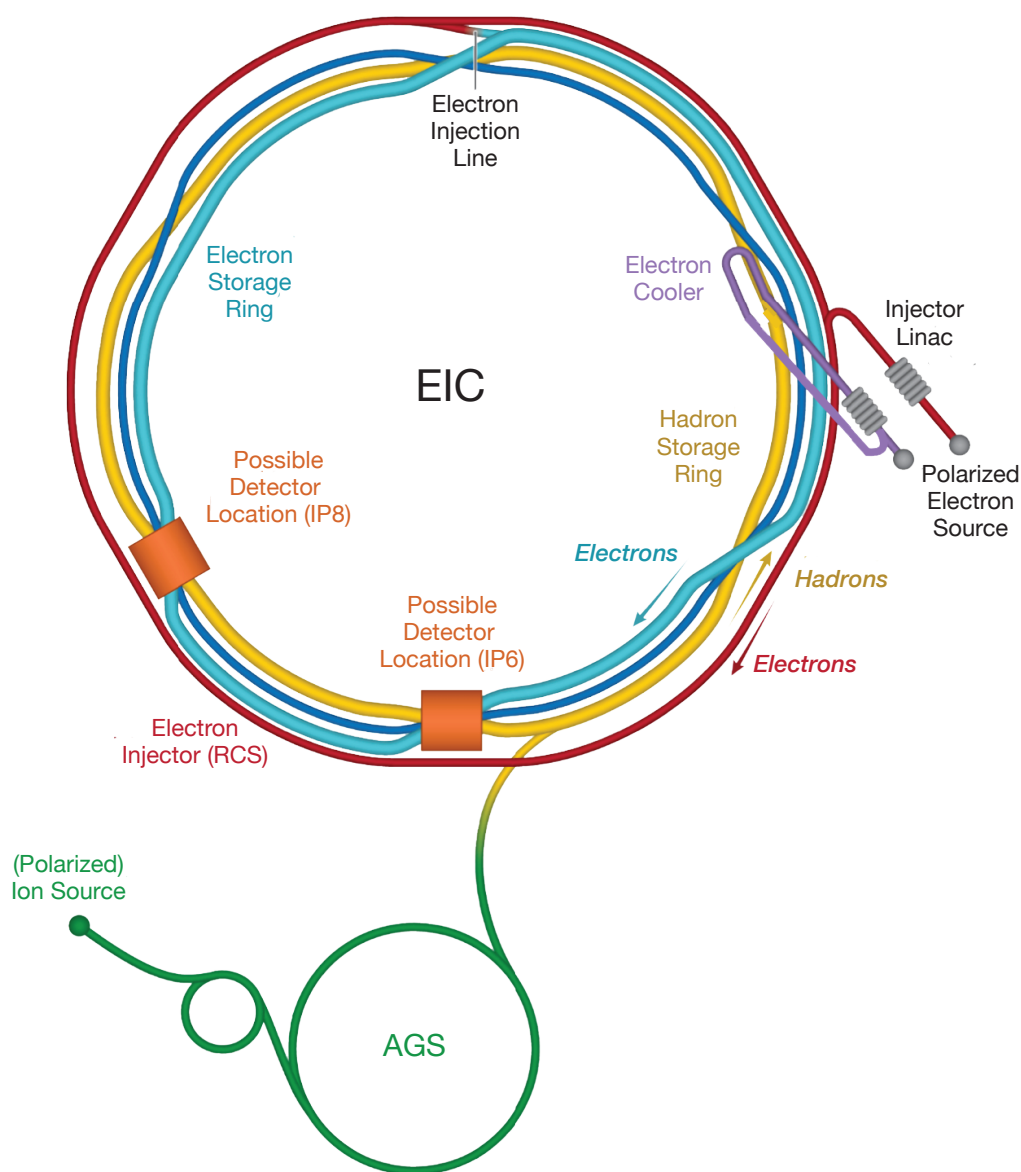


**Figure 1.1:** Schematic layout of the planned EIC accelerator based on the existing RHIC complex at Brookhaven National Laboratory.

electrons and ions and use sophisticated, large detectors to identify specific reactions whose precise measurement can yield previously unattainable insight into the structure of the nucleon and nucleus. The EIC will open a new window into the quantum world of the atomic nucleus and allow physicists access for the first time to key, elusive aspects of nuclear structure in terms of the fundamental quark and gluon constituents. Nuclear processes fuel the universe. Past research has provided enormous benefit to society in terms of medicine, energy and other ap-

plications. Particle accelerators and related technologies play a key role in the discovery sciences and it is estimated that about 30,000 worldwide are operating in industry. The EIC will probe the frontiers of nuclear science well into the twenty-first century using one of the world's most sophisticated particle accelerators and large detectors that will utilize cutting-edge technology.

The realization of the EIC is led jointly by Brookhaven National Laboratory and Thomas Jefferson National Accelerator Facility at Newport News, Virginia. It will involve physicists and engineers from other laboratories and universities in the U.S. and from around the world. This realization is expected to roughly take a decade, with beam operations to start in the early 2030s.

The EIC Users Group (EICUG, [www.eicug.org](http://www.eicug.org)) was founded in 2016. It now contains over 1200 members from 245 institutions located in 33 countries around the world. Late in 2019, the EICUG decided to organize an intensive, year-long consideration of the EIC physics measurements and scientific equipment by the members of the user group. This Yellow Report (YR) summarizes these studies and the conclusions that have been reached. The purpose of the Yellow Report Initiative is to advance the state and detail of the documented community physics studies (EIC White Paper, Institute for Nuclear Theory program proceedings) and detector concepts (Detector and R&D Handbook) in preparation for the realization of the EIC. The effort aims to provide the basis for further development of concepts for experimental equipment best suited for science needs, including complementarity of two detectors towards future Technical Design Reports. It is expected that this YR will be the cornerstone on which detector proposals will be developed by user collaborations beginning in 2021.

The work reported on here was organized by the EICUG at an in-person meeting in December 12-13, 2019 at the Massachusetts Institute of Technology, Cambridge, Massachusetts and was structured around four subsequent meetings in 2020: March 19-21, 2020 at Temple University, Philadelphia; May 20-22, 2020 at University of Pavia, Pavia, Italy; September 16-18, 2020 at the Catholic University of America, Washington, DC and November 19-21, 2020 at the University of California, Berkeley. This was a massive, international, sustained effort through the year 2020 and was overseen by 8 conveners and 41 sub-conveners. Because of the restrictions due to the pandemic, all of the EICUG meetings and interactions in 2020 were carried out remotely.

The EIC will be one of the largest and most sophisticated new accelerator projects worldwide in the next few decades, and the only planned for construction in the United States. It will address profound open questions in the fundamental structure of matter and attract new generations of young people into the pursuit of careers in science and technology. Its high design luminosity and highly polarized beams are beyond state-of-the-art and its realization will likewise push the frontiers of particle accelerator science and technology.

## Chapter 2

# Physics Measurements and Requirements

### 2.1 Introduction

The Electron-Ion Collider (EIC) will address some of the most fundamental questions in science regarding the visible world, including the origin of the nucleon mass, the nucleon spin, and the emergent properties of a dense system of gluons. The science program has been reviewed by the National Academy of Sciences (NAS) which concluded that "the EIC science is compelling, fundamental, and timely." [1]. The NAS review was based on a series of workshops hosted by the Institute of Nuclear Theory (INT) culminating in a whitepaper in 2012 and an update in 2014 entitled "Understanding the glue that binds us all" [2]. The desire and need to construct a new collider facility were prominently featured in the 2015 US Long-Range Plan for Nuclear Science [3].

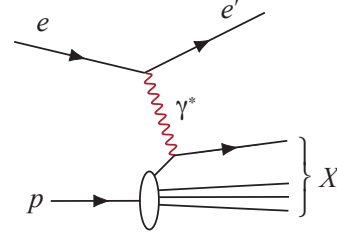
In this executive section, we present a selection of crucial physics topics that led to the recommendation for the construction of an EIC, and summarize the machine parameters and detector requirements needed to address them.

Key science questions that the EIC will address are:

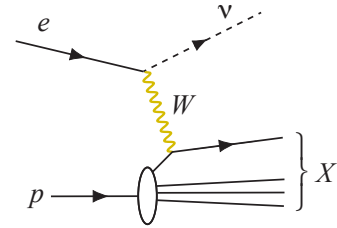
- How do the nucleonic properties such as mass and spin emerge from partons and their underlying interactions?
- How are partons inside the nucleon distributed in both momentum and position space?
- How do color-charged quarks and gluons, and jets, interact with a nuclear medium? How do the confined hadronic states emerge from these quarks and gluons? How do the quark-gluon interactions create nuclear binding?

**Table 2.1:** Different categories of processes measured at an EIC (Initial state: Colliding electron ( $e$ ), proton ( $p$ ), and nuclei ( $A$ ). Final state: Scattered electron ( $e'$ ), neutrino ( $\nu$ ), photon ( $\gamma$ ), hadron ( $h$ ), and hadronic final state ( $X$ )).

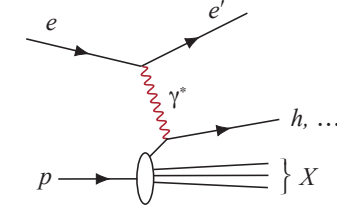
**Neutral-current Inclusive DIS:**  $e + p/A \rightarrow e' + X$ ; for this process, it is essential to detect the scattered electron,  $e'$ , with high precision. All other final state particles ( $X$ ) are ignored. The scattered electron is critical for all processes to determine the event kinematics.



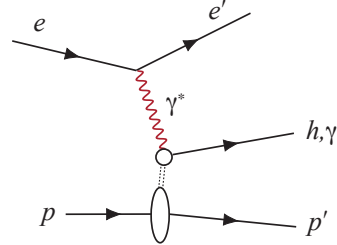
**Charged-current Inclusive DIS:**  $e + p/A \rightarrow \nu + X$ ; at high enough momentum transfer  $Q^2$ , the electron-quark interaction is mediated by the exchange of a  $W^\pm$  gauge boson instead of the virtual photon. In this case the event kinematic cannot be reconstructed from the scattered electron, but needs to be reconstructed from the final state particles.



**Semi-inclusive DIS:**  $e + p/A \rightarrow e' + h^{\pm,0} + X$ , which requires measurement of *at least one* identified hadron in coincidence with the scattered electron.



**Exclusive DIS:**  $e + p/A \rightarrow e' + p'/A' + \gamma/h^{\pm,0}/VM$ , which require the measurement of *all* particles in the event with high precision.



- How does a dense nuclear environment affect the dynamics of quarks and gluons, their correlations, and their interactions? What happens to the gluon density in nuclei? Does it saturate at high energy, giving rise to gluonic matter or a gluonic phase with universal properties in all nuclei and even in nucleons?

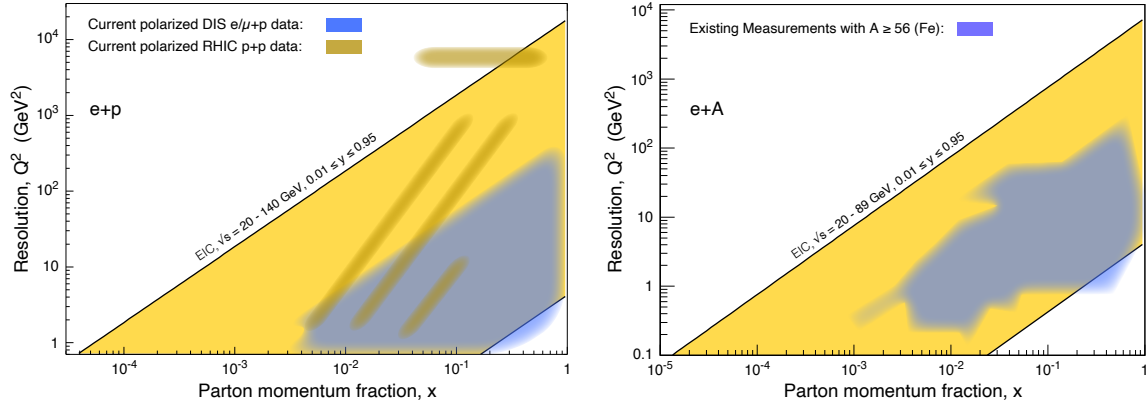


**Figure 2.1:** Left: The  $x$ - $Q^2$  range covered by the EIC (yellow) in comparison with past and existing polarized  $e/\mu+p$  experiments at CERN, DESY, JLab and SLAC, and  $p+p$  experiments at RHIC. Right: The  $x$ - $Q^2$  range for  $e+A$  collisions for ions larger than iron (yellow) compared to existing world data.

The EIC covers a center-of-mass energy range for  $e+p$  collisions of  $\sqrt{s}$  of 20 to 140 GeV. The kinematic reach in  $x$  and  $Q^2$  is shown in Figure 2.1. The quantities  $x$ ,  $y$ , and  $Q^2$  are obtained from measurements of energies and angles of final state objects, i.e. the scattered electron, the hadronic final-state or a combination of both. The quantity  $x$  is a measure of the momentum fraction of the struck parton inside the parent-proton.  $Q^2$  refers to the square of the momentum transfer between the electron and proton and is inversely proportional to the resolution. The diagonal lines in each plot represent lines of constant inelasticity  $y$ , which is the ratio of the virtual photon's energy to the electron's energy in the target rest frame. The variables  $x$ ,  $Q^2$ ,  $y$  and  $s$  are related through the equation  $Q^2 \simeq sxy$ . The left figure shows the kinematic coverage for polarized and unpolarized  $e+p$  collisions, and the right figure shows the coverage for  $e+A$  collisions. The EIC will allow in both collider modes an important overlap with present and past experiments. In addition, the EIC will provide access to entirely new regions in both  $x$  and  $Q^2$  in a polarized  $e+p$  collider and  $e+A$  collider mode, such as the low- $x$  region, providing critical information about the gluon-dominated regime.

Volume 2 of this Yellow Report provides a detailed overview of the EIC physics program, including several recent developments not addressed in the EIC White Paper. In what follows, we focus on the most critical aspects of the scientific questions outlined above and motivate the machine and detector parameters needed to address these questions.

## 2.2 Origin of Nucleon Spin

Understanding the nucleon spin in terms of contributions from quark and gluon spin and angular momentum contributions has been an essential goal for nuclear scientists for several decades. The nucleon spin can be split into its components according to [4]

$$\frac{1}{2} = \frac{1}{2}\Delta\Sigma(\mu) + \Delta G(\mu) + L_{Q+G}(\mu), \quad (2.1)$$

where  $\Delta\Sigma$ ,  $\Delta G$ , and  $L$  are the contributions from the quark plus antiquark spin, the gluon spin, and the parton angular momenta, respectively. All terms of this spin decomposition depend on the renormalization scale  $\mu$ . The parton spin contributions follow from the respective helicity distributions upon integration over the whole  $x$ -range from 0 to 1. The discovery by the EMC experiment at CERN in the 1980s that the  $\Delta\Sigma$  term can only explain a small fraction of the nucleon spin brought this topic into the limelight. Numerous fixed-target polarized electron/muon DIS experiments and polarized  $p+p$  experiments at RHIC [5], covering the range  $0.005 \lesssim x \lesssim 0.6$ , not only confirmed the general finding of the EMC experiment but also suggest that  $\Delta G$  is not large enough to make up the missing contribution to the nucleon spin, thus providing a clear indication of a nonzero orbital angular momentum contribution. However, the numerical values for  $\Delta\Sigma$  and  $\Delta G$  have large uncertainties because, thus far, we have no information at all about the parton helicity distributions for  $x \lesssim 0.005$ . With measurements in this kinematic region combined with precision measurements over the full kinematic range accessible to EIC, the EIC will drastically reduce these uncertainties. Therefore, the EIC will put the nucleon spin decomposition's phenomenology on much firmer ground, and by inference well constrain the parton angular momenta contribution [2, 6, 7].

**Machine and detector requirements for polarized DIS** Obtaining information on  $\Delta\Sigma$  and  $\Delta G$  at the EIC requires measuring DIS with longitudinally polarized electrons and longitudinally polarized protons for a large range in  $x$  and  $Q^2$  and thus over a wide range in center-of-mass energy. One of the key detector requirements at low  $x$  refers to the precision measurement of the scattered electron's energy ( $E$ ) demanding good electromagnetic calorimetry at the level of  $\sigma(E)/E \approx 10\%/\sqrt{E} \otimes (1-3)\%$  in the central detector region and superior performance at the level of  $\sigma(E)/E \approx 2\%/\sqrt{E} \otimes (1-3)\%$  in the backward or rear direction. In addition, robust electron/hadron separation is essential. The reconstruction of kinematic variables at higher  $x$ -values including the hadronic final state requires good momentum resolution and calorimetric measurement, in particular in the forward direction. Radiative corrections need to be properly addressed, both in terms of theoretical treatment and experimental design.

## 2.3 Origin of Nucleon Mass

More than 99% of the mass of the visible universe resides in atomic nuclei, whose mass, in turn, is primarily determined by the masses of the proton and neutron. Therefore, it is of utmost importance to understand the origin of the proton (and neutron) mass, particularly how it emerges from the strong interaction dynamics. Interestingly, the proton mass is not even approximately given by summing the masses of its constituents, which can be attributed to the Higgs mechanism. Just adding the masses of the proton's valence quarks provides merely about 1% of the proton mass. While a QCD analysis leads to a more considerable quark mass contribution to the proton mass, the qualitative picture that the Higgs mechanism is responsible for only a small fraction of the proton mass is not altered. An essential role for a complete understanding of the proton mass is played by the trace anomaly of the QCD energy-momentum tensor [8–11]. It is precisely this essential ingredient for which the EIC can deliver crucial input through dedicated measurements of quarkonia's exclusive production ( $J/\psi$  and  $\Upsilon$ ) close to the production threshold.

Another way to address the emergence of hadron mass is through chiral-symmetry features that manifest in the lightest mesons, the pion and kaon. In this picture, the properties of the nearly massless pion are the cleanest expressions of the mechanism that is responsible for the emergence of the mass and have measurable implications for the pion form factor and meson structure functions [12]. At variance with the pion, the effects of the Higgs mechanism, which gives a non-vanishing mass to the quarks, play a more substantial role for the kaon mass due to its strange quark content. Therefore, a comparison of the charged pion and charged kaon form factors over a wide range in  $Q^2$  would provide unique information relevant to understanding the generation of hadronic mass. The EIC can also open a vast landscape of structure function measurements constraining quark and gluon energy distributions in pions and kaons.

**Machine and detector requirements for nucleon mass studies** The main physics channel to study the nucleon mass's origin is the multi-dimensional measurement of the quarkonium production cross-section near threshold, which demands high luminosity. A precise reconstruction of the scattered electron's energy at low- $Q^2$  is essential. To accurately measure the  $t$ -dependence for quarkonium production, recoil protons need to be detected, which demands a careful design of the interaction region to measure the forward-going protons scattered under small angles.



## 2.4 Multi-Dimensional Imaging of the Nucleon

Inclusive DIS provides a 1-dimensional picture of the nucleon as it reveals the  $x$ -distribution of (longitudinal) parton momenta in the direction of the nucleon momentum. However, due to confinement, the partons also have nonzero momenta in the (transverse) plane perpendicular to the nucleon momentum. The 3D parton structure of hadrons in momentum space is encoded in transverse momentum dependent parton distributions (TMDs). For both quarks and gluons inside a spin- $\frac{1}{2}$  hadron, a total of 8 leading-twist TMDs exist [13]. These functions of different correlations between spins and transverse momenta reveal different insights into the dynamics of nucleons. TMDs can be measured via certain semi-inclusive processes, such as semi-inclusive DIS (SIDIS), where one detects an identified hadron in addition to the scattered lepton.

In the past, the unpolarized SIDIS cross-section and, in particular, the so-called Sivers asymmetry have been studied for different final-state hadrons. The latter observable describes a single-spin asymmetry with a transversely polarized target, which gives direct access to the Sivers function  $f_{1T}^\perp$  [14, 15], one of the eight quark TMDs. The data sets used to constrain TMDs are currently even more limited in  $x$  and  $Q^2$  than those shown in Fig. 2.1 (left) used to constrain helicity parton distribution functions (PDFs). With its polarized beams and the large energy range, the EIC will dramatically advance our knowledge of TMDs. The 3D momentum structure of the nucleon for the different quark flavors and the gluons will be mapped out over a wide range in  $x$  and  $Q^2$  [2, 16].

An essential aspect of TMDs concerns their scale-dependence (evolution) as predicted in QCD, which is considerably more involved than the evolution of the 1D PDFs. There is, therefore, substantial interest in a quantitative understanding of the TMD evolution. The EIC will be ideal for such studies, complementing the high precision data becoming available from JLab at larger values of  $x$ .

It allows to explore SIDIS observables over an extensive range in  $Q^2$  while covering transverse momenta of the final-state hadrons over a wide range from low (non-perturbative) to high (perturbative) values.

While the current knowledge about the Sivers function in the valence region still has considerable uncertainties, the situation is even worse for sea quarks and gluons where hardly any experimental information exists. At the EIC, the gluon Sivers function can be addressed through transverse single-spin asymmetries for the production of nearly back-to-back pairs of jets or heavy-flavor hadrons. We note that, qualitatively, the above discussion of the Sivers function applies also to the other TMDs. Generally, the EIC has transformative potential in the field of the nucleon's 3D structure in momentum space.

**Machine and detector requirements for TMD measurements** Measurements of TMDs require unpolarized as well as longitudinally and transversely polarized hadron beams colliding with (un)polarized electrons. The wide range in  $x$  and  $Q^2$  provided by the EIC is essential for mapping the TMDs. SIDIS requires the identification of final-state hadrons in coincidence with the scattered electrons. Identifying hadrons allows one to obtain information about the flavor of quarks, which have fragmented into the hadron(s). Excellent particle identification (PID) is required to separate  $\pi/K/p$  at the level of  $3\sigma$  up to  $50\text{ GeV}/c$  in the forward region, up to  $10\text{ GeV}/c$  in the central detector region, and up to  $7\text{ GeV}/c$  in the backward region. Mapping the TMDs in multiple dimensions will require larger data samples than for fully inclusive measurements. To disentangle the flavor dependence of the various TMDs, it is essential to collect data with neutron-rich transversely polarized beams of D or  $^3\text{He}$  under equivalent experimental conditions.

## 2.5 Imaging the Transverse Spatial Distributions of Partons

As in the case of the transverse momentum distribution of partons inside a hadron, we know very little about their distribution in the transverse spatial dimensions, combined with the information about the longitudinal momentum fraction  $x$ . Those spatial distributions of partons yield a picture that is complementary to the one obtained from TMDs. So far, our level of knowledge of the spatial distributions for valence quarks, sea quarks, and gluons is still relatively low.

It is possible to determine the transverse spatial distributions of quarks and gluons experimentally, where their study requires a particular category of measurements, that of exclusive reactions. Examples are deeply virtual Compton scattering (DVCS) and deeply virtual meson production. For those reactions, the proton remains intact, and a photon or a meson is produced. Exclusivity demands that all final-state products are detected, i.e., the scattered electron, the produced photon or meson, and the scattered proton. The spatial distributions of quarks and gluons in these measurements are extracted from the Fourier transform of the differential cross-section for the momentum transfer  $t$  between the incoming and the scattered proton. The non-perturbative quantities that encode the spatial distributions are called generalized parton distributions (GPDs) [17–19]. In addition to the fundamental role of GPDs concerning the spatial distribution of partons inside hadrons [20], the second moment of particular sets of GPDs will provide more in-depth insight into the total angular momentum of quarks and gluons in the proton [21]. GPDs offer a unique opportunity to probe the energy-momentum tensor and thus open the door to deepen our understanding of the nucleon mass. Moreover, GPDs contain information about the pressure and shear forces inside hadrons [22].

Our knowledge of GPDs from DVCS is currently limited and is based on fixed-target experiments at intermediate to high- $x$  or on the HERA collider measure-

ments at low- $x$ . The polarized beams and higher luminosity at EIC, along with forthcoming data from JLab at 12 GeV, will make a very significant impact on those measurements. It is anticipated that measurements made for protons in the range  $0.04 \lesssim t < 1.5 \text{ GeV}^2$  will enable maps of parton distributions all the way down to 0.1 fm [7, 23]. Such exclusive measurements performed on nuclei will enable us to understand the transverse quark and gluon distributions within.

**Machine and detector requirements for GPD measurements** GPD physics is one of the most demanding aspects of the EIC program in terms of luminosity as it requires multi-dimensional binning of processes that have very low cross-sections. The collection of data at several center-of-mass energies to cover the physics program outlined in the EIC White Paper [2] is essential. The continuous measurement of the momentum transfer to the nucleon in the range  $0.02 \text{ GeV}^2 \lesssim |t| \lesssim 1.5 \text{ GeV}^2$  demands a careful design of the interaction region to detect the forward-going protons scattered under small angles combined with a careful choice of the hadron beam parameters, *i.e.*, angular divergence, and large acceptance magnets.

## 2.6 Physics with High-Energy Nuclear Beams at the EIC

The nucleus is a QCD molecule, with a complex structure corresponding to bound states of nucleons. Understanding the formation of nuclei in terms of QCD degrees-of-freedom is an ultimate long-term goal of nuclear physics. With its broad kinematic reach, as shown in Fig. 2.1, the capability to probe a variety of nuclei in both inclusive and semi-inclusive DIS measurements, the EIC will be the first experimental facility capable of exploring the internal 3-dimensional sea quark and gluon structure of a nucleus at low  $x$ . Furthermore, the nucleus itself is a unique QCD laboratory for discovering the collective behavior of gluonic matter at an unprecedented occupation number of gluons, for studying the propagation of fast-moving color charges in a nuclear medium to shed light on the mystery of the hadronization process, and to explore the quark-gluon origin of short range nucleon-nucleon forces in the nuclei.

A key feature of gluon saturation is the emergence of a momentum scale  $Q_s$ , known as the saturation scale. When this scale significantly exceeds the QCD confinement scale  $\Lambda_{QCD}$ , the dynamics of strongly correlated gluons can be described by weak coupling many-body methods. The framework that enables such computations is an effective field theory called the Color Glass Condensate (CGC) [24]. The CGC predicts that  $Q_s^2 \propto A^{1/3}$ ; thus, the novel domain of saturated gluon fields can be accessed especially well in large nuclei. This regime of QCD is predicted to exist in all hadrons and nuclei when boosted to high energies where one can probe the low- $x$  region in full detail. Unambiguously establishing this novel domain of QCD and its detailed study is one of the most critical EIC goals.

Multiple experimental signatures of saturation have been discussed in the literature [2]. The EIC program follows a multi-pronged approach taking advantage of the versatility of the EIC facility. One of the key signatures concerns the suppression of dihadron angular correlations in the process  $e + A \rightarrow e' + h_1 + h_2 + X$ . The angle between the two hadrons  $h_1$  and  $h_2$  in the azimuthal plane is sensitive to the transverse momentum of gluons and their self-interaction—the mechanism that leads to saturation. The experimental signature of saturation is a progressive suppression of the away-side ( $\Delta\Phi = \pi$ ) correlations of hadrons with increasing atomic number  $A$  at a fixed value of  $x$ . Diffraction and diffractive particle production in  $e+A$  scattering is another promising avenue to establish the existence of saturation and to study the underlying dynamics. Diffraction entails the exchange of a color-neutral object between the virtual photon and the proton remnant. As a consequence, there is a rapidity gap between the scattered target and the diffractively produced system. At HERA, these types of diffractive events made up a large fraction of the total  $e+p$  cross-section (10–15%). Saturation models predict that at the EIC, more than 20% of the cross-section will be diffractive. In simplified terms, since diffractive cross-sections are proportional to the square of the nuclear gluon distribution,  $\sigma \propto g(x, Q^2)^2$ , they are very sensitive to the onset of non-linear dynamics in QCD. An early measurement of coherent diffraction in  $e+A$  collisions at the EIC would provide the first unambiguous evidence for gluon saturation.

**Machine and detector requirements for studies of gluon saturation** Operation of the EIC at the highest energies with the heaviest nuclei will be an essential requirement for discovering gluon saturation. Good tracking performance and forward calorimetric measurements are important in addition to very forward instrumentation of measuring diffractive events using a specialized silicon detector system known as Roman pots. Studying diffractive processes poses stringent requirements on the hermeticity of a detector system. A detailed study of saturation beyond its discovery would require a systematic variation of the nuclear size and of  $\sqrt{s}$  to see where the saturation sets in.

## 2.7 Nuclear Modifications of Parton Distribution Functions

When compared to our knowledge of parton distribution functions in the proton, our understanding of nuclear PDFs (nPDF) is significantly more limited. Most of it comes from fixed-target experiments in a region of intermediate to high- $x$  values. Recently available data from hadronic collisions at the LHC have had little impact on extracting nuclear PDFs [25]. High energy electron-nucleus collisions at the EIC will enable measurements of nuclear PDFs over a broad and continuous range in  $Q^2$ , all the way from photo-production ( $Q^2 \sim 0$ ) to high  $Q^2$  in the perturbative regime. This will lead to the study of the nPDFs with unprecedented precision and to the understanding of the collective effects that lead to modifications of nuclear

PDFs compared to a proton. How parton distributions in nuclei are modified can be quantified by plotting their ratio to parton distributions in the proton, normalized by the nucleus's atomic number. The deviation of this ratio from unity is a clear demonstration that the nuclear parton distributions are not simple convolutions of those in the proton. A ratio below unity is often called shadowing, while an enhancement is referred to as anti-shadowing.

Nuclear PDFs are determined through global fits to existing inclusive DIS data off nuclei. These are the structure function  $F_2$  and the longitudinal structure function  $F_L$ . While  $F_2$  is sensitive to the momentum distributions of (anti-)quarks and gluons mainly through scaling violations,  $F_L$  has a more considerable direct contribution from gluons. Note that the measurement of  $F_L$  requires one to operate the collider at several different center-of-mass energies.

An additional constraint on the gluon distribution at moderate to high- $x$  comes from charm production via photon-gluon fusion. The fraction of charm production grows with the energy, reaching about  $\sim 15\%$  of the total cross-section at the highest  $\sqrt{s}$ , thus permitting one to set a robust and independent constraint on the gluon distribution in nuclei at high- $x$  [2,7].

**Machine and detector requirements for precision nuclear PDF measurements** Based on recent studies for inclusive DIS and charm cross-section measurements [26], large  $\sqrt{s}$  provides access to a broader  $x$ - $Q^2$  coverage and reaches more in-depth into the small- $x$  regime of gluon dominance. Measurements involving charm-final states require good impact parameter resolution at the level of  $\sigma_{xy} \sim 20/p_T \otimes 5 \mu\text{m}$ . The general detector requirements are similar to inclusive and semi-inclusive measurements.

## 2.8 Passage of Color Charge Through Cold QCD Matter

In the standard regime of perturbative QCD at high  $Q^2$  and moderate to high  $x$ , in  $e+A$  scattering events, the virtual photon transmits a large fraction of the electron's energy. It interacts with a quark from a nucleon in the nucleus. The struck quark will subsequently traverse the nucleus, interacting with the color charges within, and continually lose energy. At some point, this quark will hadronize and form a color-neutral hadron. Whether the hadronization process happens inside or outside the nucleus depends on the interplay between the quark's energy and the atomic number of the nucleus. If the virtual photon energy (in the nuclear rest frame) is high, the quark kicked out of the nucleon will have considerable energy and produce a jet. Measuring the jets experimentally provides several advantages over studies of leading hadrons. Reconstructed from multiple (ideally all) final state particles produced by hadronization of the scattered parton, jets are much closer proxies for the parton kinematics than any single-particle observable. Us-

ing jets in many cases removes (or minimizes) hadronization uncertainties. On the other hand, jets are composite objects with rich internal substructure encoding shower evolution and hadronization details.

At the EIC, the production of jets will be a useful tool to measure and study the hadronic component in high energy photon structure [27] and gluon helicity in polarized protons [7]. Jet measurements will also constrain polarized and unpolarized parton distribution functions, probing gluon transverse momentum dependent distributions, contribute to studies of QCD hadronization, shower evolution, and cold nuclear matter effects. An energetic jet from a scattered parton encodes the history of multiple interactions with the target nucleus, which generate  $p_T$ -broadening. Thus, a comparison of the cross-section in  $e+p$  and  $e+A$  collisions is expected to be sensitive to in-medium broadening effects. Several key measurements relying on jets were identified for their sensitivity to parton energy loss in the nucleus [28], together with the development of new tools for controlling hadronization effects. Among such measurements are several variables assessed via lepton-jet correlations, including the electron's ratio to jet transverse momenta and a relative azimuthal angle between the measured jet and electron. These measurements will constrain the parton transport coefficient in nuclei [29]. It is expected that the variability of the collider's energy and the "dialing" of the nuclear size will allow us to study both the emergence of jets as a function of energy and the internal spatial structure of jets systematically as an additional topic of high interest.

In addition to jet studies, identified hadron measurements will provide additional experimental avenues for a detailed understanding of cold-QCD effects of color-charge. Parton propagation through cold nuclear matter and its' effects on hadronization have been previously studied by the HERMES collaboration in semi-inclusive deep-inelastic scattering on nuclei via relative hadron production cross-sections for various light-flavor particle species.

In addition to inclusive hadron and jet production measurements, mapping the modification of heavy flavor production in reactions with nuclei of different sizes will provide an experimental handle for understanding the transport properties of nuclear matter.

**Machine and detector requirements for jets studies** Jets can only be produced and identified cleanly at high enough center-of-mass energies. High momentum jets feature higher hadron multiplicity and a more complex internal structure. As such, high center-of-mass energy is vital for jet studies. Nuclear size is an essential control variable in these experiments and a broad range from light to heavy nuclei is desired for systematic studies of energy loss in a nuclear medium. It is imperative to have matching beam energies for  $e+p$  and  $e+A$  collisions to avoid extrapolation-related uncertainties and deliver the most precise measurements of nuclear effects. One of the key detector specifications results from jet measurements requiring

good tracking performance and good calorimetric resolution. At forward rapidity hadronic final state energies are very large and require good hadronic resolution at the level of  $\sigma(E)/E \approx 50\%/\sqrt{E} \otimes 10\%$ .

## 2.9 Connections to Other Fields

EIC-based science is broad and diverse. It runs the gamut from detailed investigation of hadronic structure with unprecedented precision to explorations of new regimes of strongly interacting matter. EIC science can be characterized by a few distinguishing themes that reflect the major challenges facing modern science today, and that have deep links to cutting edge research in other subfields of physics.

A prominent example are the various opportunities for electro-weak (EW) and beyond the standard model (BSM) physics. Achieving heightened sensitivity to various BSM scenarios requires a variety of improvements including crucial constraints on the parton distributions. By recording copious high-precision data, the EIC has the potential to provide the much-needed precision at large- $x$ , with further implications for precision QCD and EW theory in  $p+p$  collisions at the LHC. But the connections reach much further. Precision measurements at the EIC can provide new limits on various BSM couplings. For example, measurements at the EIC over a wide range of  $Q^2$  will test the running of Weinberg's weak mixing-angle. The availability of polarized electron (or positron) beams with proton or deuteron targets can scrutinize lepton flavor violation mechanisms in the charged lepton sector. Furthermore, the high energy and luminosity at the EIC offers opportunities for new particle searches such as a heavy photon or a heavy neutral lepton.

Measurements at the EIC are also expected to deliver important input for several areas of astroparticle physics. Fields such as cosmic-ray air showers and neutrino astrophysics will benefit from better constrained models of hadronic interactions. Deeply inelastic scattering and photo-nuclear processes have natural ties with the physics of hadronic collisions. These relate to the issue of small- $x$  gluons and factorization in  $e+p$  and  $e+A$  versus  $p+p$  and  $p+A$ , and to the implications of the determination of parton distributions for  $p+A$  collision for an improved understanding of the initial conditions in heavy-ion collisions. Similar, the accurate characterization of parton distributions in nuclei provided by the EIC can directly benefit the neutrino physics program. In return, neutrino scattering can help better understand the parton structure of nucleons and nuclei, where the nucleon strangeness content is one example.

Even though the EIC is a high-energy collider with typical energy scales in the tens-to-hundred of GeV range, there are key measurements that are of relevance to nuclear physics at much lower energies in the tens-to-hundreds MeV range. In diffractive deep inelastic scattering at high energies, a clean separation develops

between the fragmentation region of the electron and that of the nuclear target. Correlations amongst nucleons in the target fragmentation region have the potential to provide novel insight into the underlying quark-gluon correlations that generate short-range nuclear forces. Short-range nucleon-nucleon correlations dominate the high momentum tails of the many-body nuclear wave function and show signs of universal behavior in nuclei. On the other hand, accurate nuclear structure input is needed in coherent exclusive channels with light ions — enabling the study of nuclear tomography in partonic degrees of freedom — and in reactions with spectator tagging, which result in additional control over the initial nuclear configuration.

## 2.10 Summary of Machine Design Parameters

Here we summarize the machine requirements that were motivated in the previous sections through a set of critical measurements that reflect the highlights of the EIC science program. The successful scientific outcome of the EIC depends critically on: (a) the luminosity, (b) the center-of-mass energy, and its range, (c) the lepton and light-ion beam polarization, and (d) the availability of ion beams from deuterons to the heaviest nuclei. Two interaction regions are desired to ensure a robust physics program with complementary detector systems.

**Luminosity** The EIC is being designed to achieve peak luminosities between  $10^{33}\text{cm}^{-2}\text{s}^{-1}$  and  $10^{34}\text{cm}^{-2}\text{s}^{-1}$ . To put these numbers into context, note that a luminosity of  $10^{33}\text{cm}^{-2}\text{s}^{-1}$  with strong hadron cooling ( $L_{\text{peak}} = L_{\text{avg}}$ ) yields an integrated luminosity of  $1.5\text{fb}^{-1}$  per month. Here we assume a 60% operation efficiency for the collider complex as routinely achieved by RHIC. Without strong hadron cooling for the same operation's parameters, one would get a 30% reduction, as the average luminosity  $L_{\text{avg}}$  per fill is reduced to 70% of the peak luminosity  $L_{\text{peak}}$ . Most of the key physics topics discussed in the EIC White Paper [2] are achievable with an integrated luminosity of  $10\text{fb}^{-1}$  corresponding to 30 weeks of operations. One notable exception is studying the spatial distributions of quarks and gluons in the proton with polarized beams. These measurements require an integrated luminosity of up to  $100\text{fb}^{-1}$  and would therefore benefit from an increased luminosity of  $10^{34}\text{cm}^{-2}\text{sec}^{-1}$ . It should be noted that many measurements can be performed simultaneously by judiciously choosing beam species and their spin orientation appropriately.

**Center-of-Mass Energy** To ensure a wide kinematic reach and a large coverage of phase space, the EIC requires a variable center-of-mass energy  $\sqrt{s}$  in the range of  $\sim 20 - 100\text{GeV}$ , upgradable to  $140\text{GeV}$  [2]. An energy of  $\sqrt{s_{eN}} = 140\text{GeV}$  is needed to provide sufficient kinematic reach into the gluon dominated regime.



Some measurements require a variation in  $\sqrt{s}$ . The lower center-of-mass energy limit is driven by the ability to measure transverse quantities well, which are of the order of 10-100 MeV. This is important, for example, for the accurate determination of quark TMDs at high values of  $Q^2$ .

**Polarization of beams** EIC Physics involves two types of asymmetries: (i) double-spin asymmetries, requiring both electron and hadron beams to be polarized, and (ii) single-spin asymmetries, requiring only one beam—typically the hadron beam—to be polarized. The statistical uncertainties for spin asymmetries are strongly affected by the degree of polarization achieved. For double-spin asymmetries the dependence is  $1/[P_e P_p \sqrt{N}]$  and for single-spin asymmetries it is  $1/[P \sqrt{N}]$ . Therefore, high beam polarizations are mandatory to reduce the statistical uncertainties. Measurements require longitudinal and transverse polarization orientation for protons, deuterons,  $^3\text{He}$ , and other polarizable light nuclei, as well as longitudinal polarization for the electron beam.

**Nuclear Beams** Ion beams of heavy nuclei (Gold, Lead, or Uranium) combined with the highest  $\sqrt{s}$ , will provide access to the highest gluon densities and to an understanding of how colored particles propagate through nuclear matter. On the other hand, light ions are essential to study the A-dependence of gluon saturation and for precision studies of short-range nuclear correlations.

## 2.11 Summary of Detector Requirements

The diverse physics program promised by the new Electron-Ion Collider poses a technical and intellectual challenge for the detector design to accommodate multiple physics channels. Accommodating the needs of experimental measurements with different and, at times, competing requirements in one general-purpose detector design requires detailed consideration of the physics processes involved. Preliminary investigations on this topic were put forward in the EIC White Paper [2]. Further developing a more detailed set of physics-driven requirements for a future conceptual design of a general-purpose EIC detector and considerations for a second complementary detector to overcome the technical and intellectual challenges were the primary focus of the year-long Yellow Report EIC Users Group community effort.

Figure 2.2 illustrates the correlation between polar angle ( $\theta$ ) and pseudorapidity ( $\eta = -\ln \tan(\theta/2)$ ) and the  $x - Q^2$  phase space for the EIC physics program. Recent studies of the physics-driven detector requirements were organized by three basic types DIS processes: Inclusive DIS both in neutral and charged current mode,

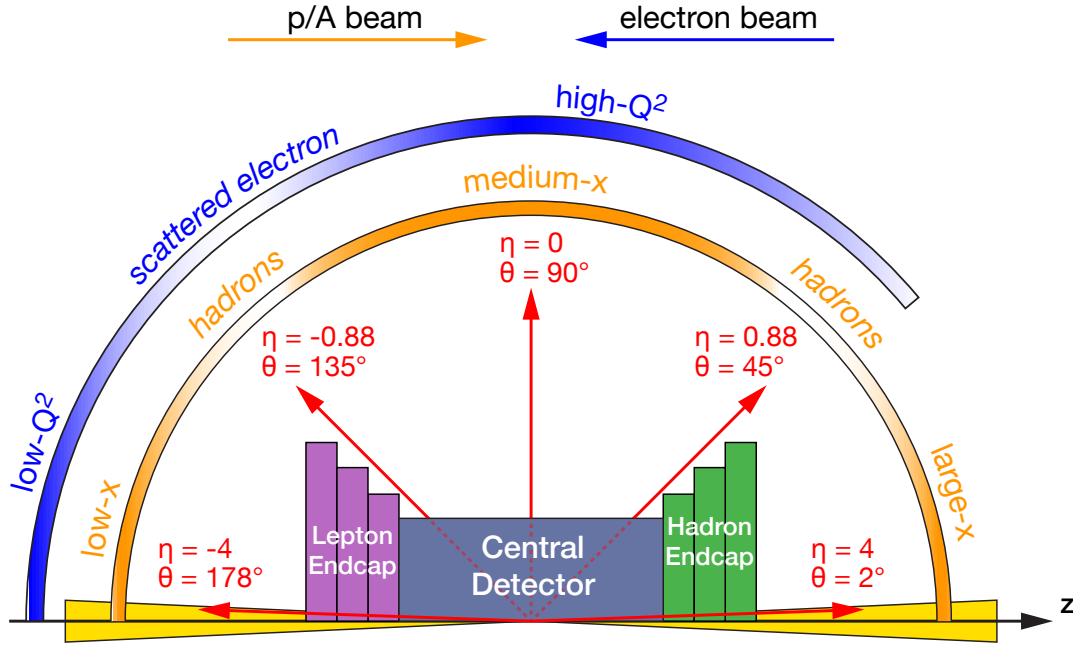


**Figure 2.2:** Schematic showing the distribution of the scattered lepton and hadrons for different  $x - Q^2$  regions over the detector polar angle / pseudorapidity coverage.

semi-inclusive DIS, and exclusive DIS. Those basic processes are shown in Table 2.1. For the following summary, and throughout this document, the beams' directions follow the convention used at the HERA collider at DESY: the hadron beam travels in the positive  $z$ -direction/pseudorapidity and is said to be going "forward." The electron beam travels in the negative  $z$ -direction/pseudorapidity and is said to be going "backward" or in the "rear" direction.

All physics processes to be measured at an EIC require having the event and particle kinematics  $(x, Q^2, y, W, p_t, z, \phi, \theta)$  reconstructed with high precision. Kinematic variables such as  $x$ ,  $Q^2$ ,  $y$ , and  $W$  can be determined from the scattered electron or the hadronic final state using the Jacquet-Blondel method [30] or a combination of both. The electron method provides superior resolution performance for  $x$  and  $y$  in the low  $x$  region, while the Jacquet-Blondel method yields increased resolution performance for  $x$  and  $y$  towards large  $x$  values. To access the full  $x - Q^2$  plane at different center-of-mass energies and for strongly asymmetric beam-energy combinations, the detector must be able to reconstruct events over a wide span in polar angle ( $\theta$ ) and pseudorapidity ( $\eta$ ). This imposes stringent requirements on both detector acceptance and the resolution of measured quantities such as the energy and polar angle in the electron-method case.

**Detector Requirements** Below we summarize the critical detector requirements that are imposed by the rich physics program of an EIC.

- The EIC requires a  $4\pi$  hermetic detector with low mass inner tracking.
- The primary detector needs to cover the range of  $-4 < \eta < 4$  for the measurement of electrons, photons, hadrons, and jets. It will need to be augmented by auxiliary detectors like low- $Q^2$  tagger in the far backward region and proton (Roman Pots) and neutron (ZDC) detection in the far forward region.
- The components of an EIC detector will have moderate occupancy as the event multiplicities are low. However, specific components close to the beam-line might see higher occupancies depending on the machine background level.
- Compared to LHC detectors, the various subsystems of an EIC detector have moderate radiation hardness requirements.
- Excellent momentum resolution in the central detector ( $\sigma_{p_T}/p_T(\%) = 0.05p_T \otimes 0.5$ ).
- Good momentum resolution in the backward region with low multiple-scattering terms ( $\sigma_{p_T}/p_T(\%) \approx 0.1p_T \otimes 0.5$ ).
- Good momentum resolution at forward rapidities ( $\sigma_{p_T}/p_T(\%) \approx 0.1p_T \otimes (1 - 2)$ ).
- Good impact parameter resolution for heavy flavor measurements ( $\sigma_{xy} \sim 20/p_T \otimes 5 \mu\text{m}$ ).
- Good electromagnetic calorimeter resolution in the central detector ( $\sigma(E)/E \approx 10\%/\sqrt{E} \otimes (1 - 3)\%$  at midrapidity).
- Excellent electromagnetic calorimeter resolution at backward rapidities ( $\sigma(E)/E \approx 2\%/\sqrt{E} \otimes (1 - 3)\%$ ).
- Good hadronic resolution in the forward region ( $\sigma(E)/E \approx 50\%/\sqrt{E} \otimes 10\%$ ).
- Excellent PID for  $3\sigma \pi/K/p$  separation up to  $50 \text{ GeV}/c$  in the forward region, up to  $10 \text{ GeV}/c$  in the central detector region, and up to  $7 \text{ GeV}/c$  in the backward region.

Volume 2 of this Yellow Report provides further details on the detector requirements and a detailed discussion of the achievable precision for various observables.

The EIC physics program will allow us to deepen our understanding of the visible world around us, including the origin of the nucleon mass, the nucleon spin,

and the emergent properties of a dense system of gluons. This program requires a unique and versatile accelerator facility of colliding polarized electron and polarized proton and light-ion beams, and a range of light and heavy nuclei. The broad variety of processes required to address the diversity of the EIC science program similarly demands a unique  $4\pi$  hermetic, asymmetric detector systems capable of identifying and reconstructing the energy and momentum of final-state particles with high precision.

## Chapter 3

# Detector Concepts

EIC detectors are essential to make the detailed measurements described in the previous section to access the physical observables described by theoretical calculations. They will be large, sophisticated, and unique instruments which will be designed and constructed by multi-institutional collaborations of the EIC users from laboratories and universities around the world. This effort profits from a wealth of experience gained at the first  $e+p$  collider facility HERA at DESY, Germany and the enormous development of novel detector concepts over the last several decades, since the first  $e+p$  collisions at HERA in 1992. The detectors will be located at the interaction regions, where the electron and ion beams are brought into collision in a controlled way. The 2015 US Nuclear Physics Long Range Plan recommended consideration of multiple EIC interaction regions and the EIC users have clearly stated their desire for two EIC detectors to effectively carry out the extensive scientific program.

The EIC detectors must be located in the interaction regions where space is constrained due to the requirements of high luminosity. They must have strong integration of forward and backward detectors and multiple hermetic functionalities (precision energy measurement and particle tracking and identification) to determine the energy-momentum four-vector of final-state particles over a large range of energies:  $\sim 10$  MeV to  $\sim 10$  GeV.

In addition to the major detector facilities, other sophisticated scientific instrumentation will be essential to carry out the scientific program. The collision luminosity must be determined using special purpose detectors close to the beams. Furthermore, in spin-dependent measurements, precise knowledge of the polarizations of the electron and ion beams is essential. This is obtained using special purpose polarimeters which are developed and operated by separate teams of physicists, engineers, and technicians.

The design for detector(s) at the EIC is centered around solenoidal superconducting magnets with bipolar fields, which can be achieved either through improve-

ment modifications of the BABAR/sPHENIX magnet at 1.5 T or with a new superconducting magnet at 3 T. The solenoidal configuration naturally leads to tracking and vertexing, particle identification, and calorimetry systems organized in a configuration with barrel and endcap detectors. The detectors must be designed to operate with high efficiency in the presence of a large rate of background generated by the intense, circulating beams as they traverse the vicinity of the detectors.

In contrast to symmetric  $ee$  and  $pp$  colliders, the asymmetric nature of collisions at the EIC leads to unique detector requirements. The hadron endcap, barrel, and electron endcap detector systems see very different particle distributions, in terms of both momentum and particle types. Likewise, the performance requirements on these detector systems vary significantly between the detector regions. This is reflected by the critical detector requirements for the track, vertex, and energy resolution and particle identification separation summarized in the previous section.

The tracking and vertexing, particle identification, and calorimetry concepts described in this section do not identify a specific technology that can be used in all detector regions. Rather, the aim is to combine the best technology for each region in detector concepts that achieve the full set of requirements.

Multiple combined detector concepts for each detector functions are presented in this report. The complementarity between the detector technologies used in different detector concepts can be used to tailor detectors in the different interaction regions shown in Figure 1.1, at the locations of the current STAR and sPHENIX detectors.

### 3.1 Tracking and Vertexing Detector Systems

The tracking and vertexing systems under consideration are based on semiconductor detector technologies and gaseous tracking detector technologies, with concept detectors combining both technologies.

Silicon semiconductor-based sensors collect electron/hole pairs caused by the passage of charged particles. The tracking and vertexing detector systems must have high granularity to satisfy the tracking (vertexing) resolution requirements of better than  $5\ \mu\text{m}$  (around  $3\ \mu\text{m}$ ) while maintaining a low material budget below 0.8% (0.1%) of a radiation length in the barrel (endcap). Monolithic active pixel sensors (MAPS) have seen an evolution from the 180 nm technology used by STAR and ALICE to the 150/180 nm Depleted MAPS (D-MAPS). A third generation 65 nm process is under development as a joint effort between the EIC and ALICE ITS3 vertex tracker upgrade.

In gaseous tracking chambers the ionization caused by tracks drifts to anode planes in endcaps where it is collected, potentially after additional amplification. A double-sided time projection chamber (TPC) with a central cathode plane and

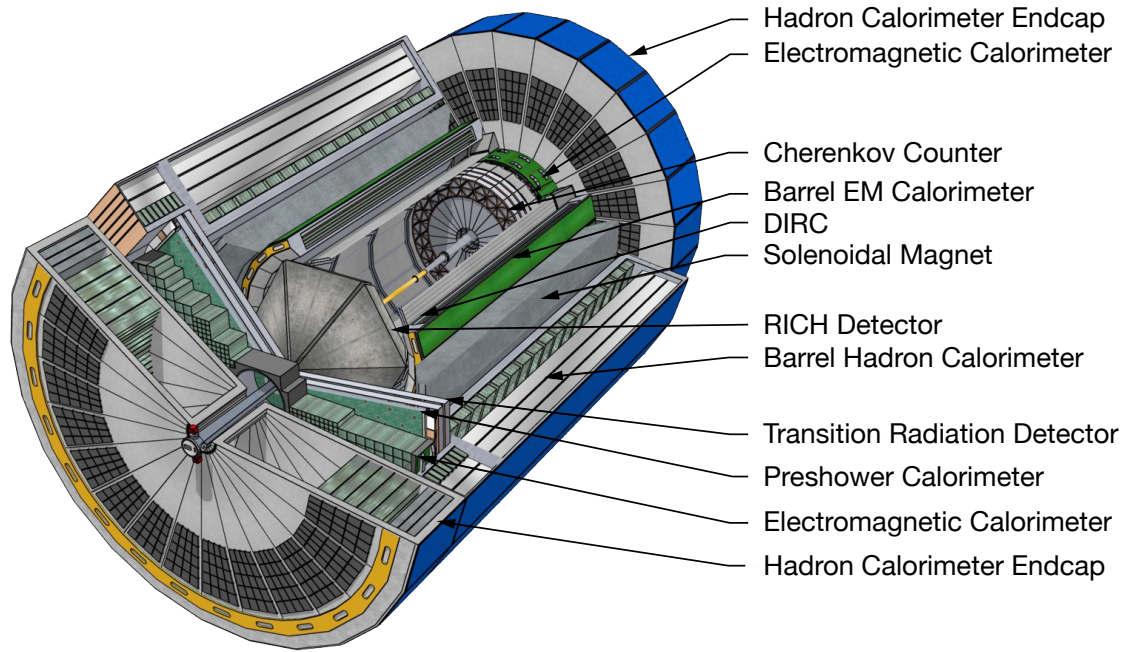


**Figure 3.1:** CAD model of a particular EIC detector concept, with the artistic rendering of the tracking, particle identification, and calorimetry subsystems.

gas amplification modules at the endcaps is under construction for the sPHENIX experiment and may be modified for use at the EIC. Upgrades to the read-out pads for the EIC would be focused on micro-pattern gaseous detectors such as gas electron multipliers (GEMs),  $\mu$ MEGAs or  $\mu$ RWELL can provide electron amplification before read-out on high granularity anode printed circuit boards. Gaseous tracking detectors also aid in particle identification with ionization energy loss information.

Two baseline tracking detector concepts are presented. An all-silicon tracking detector option with barrel and endcap silicon detector can be realized in a compact form. A hybrid tracking system combines a silicon vertex detector within a TPC and provides  $dE/dx$  measurements that can aid particle identification. In both main options, alternative tracking options exist in the backward and forward tracking endcaps.

## 3.2 Particle Identification Detector Systems

The second major detector system, particle identification, separates electrons from pions, kaons, and protons, with significant pion/electron suppression and better than  $3\sigma$  pion/kaon/proton separation in all rapidity regions. Using the specific ionization ( $dE/dx$ ) in time projection chambers with novel gas mixtures allows for improved resolution approaching the limit of Poisson statistics. However, dedi-

cated particle identification detectors, based on Cerenkov light emission and time of flight measurements will be required.

In Cerenkov detectors light emitted by tracks faster than the speed of light in a gas, aerogel, or quartz radiator medium is detected. The tight integration with the tracking system exists here as well, since the originating track must be well known. Different radiator media are required in the electron endcap, barrel, and hadron endcap due to the different momentum ranges of particles in those regions. A hadron blind detector without focusing and with CsI photocathodes evaporated on GEMs can separate electrons from hadrons. A similar detection approach with focusing is used in the CsI ring imaging Cerenkov (CsI RICH) detector. Novel approaches that use nano diamond powder instead of CsI are also under consideration. A dual RICH (dRICH) with both a gas and aerogel radiator avoids the holes in the performance due to the Cerenkov thresholds. A modular RICH (mRICH) concept uses a Fresnel lens for focusing. Finally, detection of internally reflected Cerenkov light (DIRC) is under consideration for a high performance DIRC (hpDIRC), and would outperform the DIRC at BaBar and PANDA.

Other particle identification technologies are under development as well. Time of flight particle identification at low momentum can be reached through precision timing measurements in large area picosecond photon detectors (LAPPD) in the endcaps. GEM transition radiation detectors (GEM-TRD) combined with neural networks have also been shown to separate electrons and pions.

Based on these particle identification technologies, several combined concepts are presented. The forward direction includes a gas-based Cerenkov detector but requires another technology such as the dRICH. In the central region, a combination of the DIRC and TOF detectors must be augmented with, for example, the ionization loss measurements in the hybrid tracking detector system or other identification technologies in the more compact all-silicon tracking detector system. In the backward or rear direction several options satisfy the requirements, including the mRICH with LAPPD.

### 3.3 Calorimeter Detector Systems

The third major detector system, calorimetry, measures particle energy and includes both electron and hadron calorimetry efforts. Only light-collecting calorimeters are considered here. Electromagnetic calorimetry (ECAL) requires excellent resolution to constrain the electron scattering kinematics, but also aids in separating electrons from hadrons, in the detection of neutral particles, and in the separation of the two photons from neutral pion decay. Hadron calorimetry (HCAL) is required for determination of the total energy in hadronic jets, in particular for neutral components which are not tracked.

Among possible ECAL technologies discussed are homogeneous detectors



( $\text{PbWO}_4$ , scintillating glass, and lead glass) and sampling calorimeters (scintillator fibers in tungsten powder and layered shashlyk detectors). Due to limited space available, short radiation length materials are favored. Likewise, silicon photomultipliers (SiPMs) are preferred since they take less space than regular photomultipliers and operate in the magnetic field. In the backward region,  $\text{PbWO}_4$  appears to be the only option. In the central region, projective geometry is required. In the forward region, high granularity is required to resolve pion decay photons.

For the HCAL, existing technologies (e.g. scintillating / depleted uranium sampling calorimeters as used at ZEUS) are considered sufficiently performant. Efforts are discussed to avoid lead in favor of steel, and achieve a design where the HCAL is the support structure for the ECAL. In the hadron endcap a denser material would be preferable, and the STAR Forward upgrade has allowed the construction of a small prototype of a compensating calorimeter with better resolution.

### 3.4 Auxiliary Detector Systems

In addition to the major central detector systems, specialized auxiliary detector systems will be necessary, all of which require close integration in the accelerator lattice. This is particularly true for the electron and hadron polarimeters, but also applies to the far-forward and far-backward regions of the detector.

In the far-forward region, silicon detectors in roman pots can detect very forward hadrons up to 5 mrad with high timing resolution of low gain avalanche diodes (LGADs). Similar detector technologies will be used in the off-momentum detectors to tag nuclear breakup of Lambda decay products. Neutrons and low-energy photons in the forward direction will be detected in the Zero-Degree Calorimeter (ZDC), with both ECAL and HCAL components. Technologies from the ALICE FoCal and the LHC ZDC are considered.

In the far-backward region, bremsstrahlung photons detected in an electromagnetic zero-degree calorimeter or a pair spectrometer will be used to determine the luminosity, an important normalization quantity for many observables. Very low- $Q^2$  electrons will be tagged in far-backward position-sensitive detectors or segmentation in the zero-degree calorimeter.

In other sections of the EIC, electron and hadron polarimeters will non-destructively measure the polarization to a systematic precision better than 1%. To allow timely feedback to accelerator operators, a statistical precision of similar size will be achieved on short time scales.

For the electron beam, a Compton polarimeter can reach the needed luminosity using a diode laser with high repetition frequency and a fiber amplifier to reach powers up to 20 W. To measure both longitudinal and transverse polarization, position sensitive detectors such as diamond strip or HV-MAPS detectors can be used.

For the hadron beam, the natural starting point is to use the existing polarimeters at RHIC: the atomic hydrogen jet for absolute measurements combined with a fast carbon ribbon for relative measurements. At the higher proton currents of the EIC, additional hydrogen jet detectors and alternative ribbon targets will be required. For  $^3\text{He}$  beams the hydrogen jet may be replaced by a polarized  $^3\text{He}$  target.

To manage the data acquisition bandwidth and associated selection of events of interest to the physics analyses, the EIC will use a streaming readout approach without trigger electronics that controls whether or not to record events, similar to the LHCb upgrade currently in progress. On the software side, new approaches in artificial intelligence are being explored.

### 3.5 Two Complementary Detectors

The EIC science program is diverse and broad. It requires a  $4\pi$  detector with strong integration of forward and backward detection capabilities. It requires multiple hermetic functionalities (precision energy measurement, and particle tracking and identification). It must cover a large and versatile range of energies spanning from nuclear energy scales to multi-GeV electron and ion beam energies.

The strong diversity of EIC science imposes the essential feature that the interaction region and the detector at the EIC are designed so all particles are identified and measured at as close to 100% acceptance as possible and with the necessary resolutions. Variations of the interaction region design and beam line optics between the two interaction points can allow further optimization and enhancement of EIC science reach.

The broad science reach of the EIC is also reflected in the variety of detector technologies that are under consideration. Table 3.1 summarizes the high-level performance of different subdetectors based on a 3 T solenoid for a future EIC detector. The clear conclusion is that the best way to optimize the science output is through two detectors that differ in their basic features such as the Solenoid field and choices of sub-detector technologies. This will lead to complementarity in detector acceptance and systematic effects, and presents benefits due to technology redundancy. Studies performed to date already suggest the opportunity to optimize the overall physics output of the EIC in terms of precision and kinematic range through careful complementary choices of two general purpose detectors.

In contrast to previous colliders, the complementarity between the two EIC detectors and their associated interaction regions will be built in from the start. Beyond maximizing EIC science promise, a further strong motivation for complementary detectors lies in the need for independent cross-checking of important results; the scientific community usually only becomes convinced of exciting new discoveries when two different experiments with different systematics arrive at the same conclusion.



## Chapter 4

# Opportunities for Detector Technology and Computing

In parallel with a nearly two-decade-long community effort of EIC science development and refinement, as well as experimental equipment conceptualization, BNL in association with TJNAF and the DOE Office of Nuclear Physics established in 2011 a highly successful generic EIC-related detector R&D program. This program both built bridges between various domestic and international research groups and scientific communities, and was successful in its own right towards detector R&D. Presently, 281 scientists are engaged in the generic EIC-related R&D program, from 75 institutions in 10 countries. Most of the efforts have been organizationally merged in groups of topical consortia, which can provide the seeds for the EIC detector collaboration(s).

Many of the supported projects, ongoing or completed, developed technologies that are now integral parts of existing detector concepts or are regarded as potential alternatives. The vertex detector R&D consortium aims to develop new improved Monolithic Active Pixel Sensors (MAPS) to meet the requirements demanded by the EIC requirements. Various Micro-Pattern Gas Detector (MPGD) technologies, such as Gaseous Electron Multiplier (GEM), Micromegas, and  $\mu$ RWELL, have been pursued for low material tracking in barrel and forward regions as well as Time-Projection Chamber (TPC) readouts. New concepts like miniTPCs and integrated Cherenkov-TPCs had been developed and tested. Many options for electromagnetic, and recently, hadronic calorimetry have received R&D effort within the calorimetry consortium. From this grew the Tungsten-Scintillating Fiber (W-SciFi) calorimeter, scintillating fibers embedded in a W-powder composite absorber. In parallel, novel scintillating glasses (SciGlass) have been developed with unprecedented quality as cost-effective alternative to expensive lead-tungstate ( $\text{PbWO}_4$ ) crystals. The particle identification consortium is pursuing various technologies, such as Direct-Internally Reflected Cherenkov light (DIRC) detectors, modular and Dual Ring-Imaging Cherenkov (RICH) detec-

tors, with Fresnel lens focalization in the former and with gas and aerogel radiators in the latter. New coating materials like nano-diamonds to replace Cesium-Iodide (CsI) for RICH photo sensors are also under investigation. Time-of-Flight detectors, as well as Roman Pots for forward proton detection, require highly segmented AC-coupled Low-Gas Avalanche Detector (AC-LGAD) sensors whose development has just started to get support from the program. Besides hardware R&D the program has supported various vital projects such as machine background studies and simulation software developments to enable more accurate definition of the physics' requirements. Sartre and Beagle are two examples of Monte-Carlo event generators whose development was substantially boosted by the program. Both were extensively used in the context of this report.

In general, due to this longstanding generic EIC-related detector R&D program, and further support from Laboratory Directed Research & Development (LDRD) Programs within the US national laboratories, and many university groups both inside and outside the US, the detector technologies to implement a successful comprehensive Day-One EIC Science program exist. For this reason the EIC User Group can continue to consider various technologies for many of the different detector functions to implement, with an eye also to possible detector complementarity for a second detector. The EIC also benefitted substantially from synergetic R&D conducted for many high-energy and nuclear physics experiments, not only at BNL and TJNAF, but also for experiments such as ALICE and LHCb at CERN, PANDA at GSI and BELLE-II at KEK.

On the other hand, further opportunities do remain. These are driven both by pursuing alternative detector technologies for a complementary second fully integrated EIC detector and Interaction Region, and to prepare for future cost-effective detector upgrades to enhance capabilities addressing new nuclear physics opportunities. Furthermore, the EIC will be a multi-decade nuclear physics facility after its construction is completed and will in this period likely require further detector upgrades driven by its science findings. It is expected that further physics opportunities enabled by new detector capabilities will already arise during the EIC design and construction phase.

Nuclear physics detection techniques typically need to cover a large range in energies. They can range from the MeV scale of nuclear binding energies and 100 MeV/c momentum scale below the Fermi momentum to isolate nuclear processes, all the way to the multiple tens of GeV scales to pinpoint the elementary subatomic quark-gluon processes and quark flavors. Due to this, nuclear physics drives detector technologies with often different demands than those in high-energy and particle physics. Examples are (i) particle identification techniques and their cost-effectiveness in readout (RICH, DIRC, ultra high-precision TOF, electromagnetic and hadronic calorimetry), (ii) those driving detector material minimization to detect the lowest-momentum particles (inner tracking solutions, gaseous-based radial TPCs), (iii) those pushing for specific material radiation tolerances (electro-magnetic rather than hadronic, high-power target areas, and low-energy

nuclear fragments), and (iv) those related to spin or polarization (beam, targets, polarimetry).

Further opportunities for detector technology within these overarching nuclear physics areas exist in the EIC design, construction, and science operations era. These can best be considered in detector functionality areas such as particle identification, calorimetry, tracking, and readout electronics, to address how one can enhance the performance of the EIC detector(s) with target R&D projects in a year or more.

Examples of such detector opportunities include, but are not limited to, the following: material minimization in a possible all-Silicon tracker, particle identification reach at mid rapidity and at higher momenta, cost-effectiveness of readout of particle identification detectors by improvements to Silicon Photomultipliers (SiPMs) or to Large-Area Picosecond Photo-detectors (LAPPDs). Furthermore, improvement of the achievable hadronic calorimetry resolutions, large-scale production and low-energy photon detection efficiency of possible glass-based electromagnetic calorimetry, new Application-Specific Integrated Circuit (ASIC) and front-end readout board needs required for streaming readout modes, or improved spatial and/or timing resolution of Zero-Degree Calorimeters driven by the imaging and diffractive science programs. It is crucial that some of this research for enhanced detector functionality continues and is recognized as driven by Nuclear Physics needs.

In parallel with these detector opportunities, unique opportunities exist to directly *integrate* modern computing and data analysis methods in the experiment. Efforts are underway to develop methods and production systems to establish a quasi-instantaneous high-level nuclear physics analysis based on modern statistical methods. This requires a self-calibrated matrix of detector raw data synchronized to a reference time and would remove intermediate data storage requirements. This takes direct advantage of advances in micro-electronics and computing, and of artificial intelligence (AI) methods.

Micro-electronics and computing technologies have made order-of-magnitude advances in the last decades. Combined with modern statistical methods, it is now possible to analyze scientific data to rapidly expose correlations of data patterns and compare with advanced theoretical expectations. While many existing nuclear physics and high-energy physics experiments are taking advantage of these developments by upgrading their existing triggered data acquisition to a streaming readout model (where detectors are read out continuously), these experiments do not have the opportunity of integrated systems from data acquisition through analysis, such as the EIC has. Hence, we aim to remove the separation of data readout and analysis altogether, taking advantage of modern electronics, computing and analysis techniques in order to build the next generation computing model that will be essential for probing the femto-scale science accessible at the EIC.

An integrated whole-experiment approach to detector readout and analysis to-

wards scientific output will take advantage of multiple existing and emerging technologies. Amongst these are: streaming readout, continuous data quality control and calibration, task-based high performance local computing, distributed bulk data processing at supercomputer centers, modern statistical methods that can detect differences among groups of data or associations among variables even under very small departures from normality, and systematic use of artificial intelligence (AI) methods at various stages.

To further elaborate on the latter, AI is becoming ubiquitous in all disciplines of Nuclear Physics. EIC could be one of the first large-scale collider-based programs where AI is systematically employed from the start. AI already plays an important role in existing experiments such as LHCb at CERN, where machine learning algorithms make already the majority of the near-real-time decisions what physics data should be written or proceed to a higher level analysis.

Supported by the modern electronics able to continuously convert the analog detector signals, streaming readout can further the convergence of online and offline analysis: here the incorporation of high-level AI algorithms in the analysis pipeline can lead to better data quality control during data taking and shorter analysis cycles. Indeed, AI could foster in the next years significant advances in the crucial area of fast calibration/alignment of detectors, greatly facilitating a data streaming readout approach.

For charged-particle tracking, where in nuclear physics experiments typically most of the computing cycles are spent in propagating the particles through inhomogeneous magnetic fields and material maps, AI can contribute to determine the optimal initial track parameters allowing to decrease the number of iterations needed. For particle identification, crucial for Nuclear Physics experiments, has recently seen a large growth of applications.

AI at the EIC is expected to play a role in high-level physics analysis such as searches for rare signatures which necessitates advanced techniques making strong use of machine learning to filter out events, the utilization of jets to empower taggers for boosted jets and quark flavors within the jets, and in the aid for construction of higher-level Wigner distributions from sparse and missing data. With the EIC detector design ongoing and opportunities for two detectors at the EIC, AI can be gainfully used for the design optimization process of the large and complex EIC detector systems that are based on computationally intensive simulations, for the optimization of the individual detector systems, and even the optimization of materials used within detectors for improved performance.





## Appendix A

# Deep Inelastic Scattering Kinematics

### A.1 Structure functions

In general, the inclusive DIS process can be written as

$$e(l) + N(p) \rightarrow e(l') + X(p_X), \quad (\text{A.1})$$

where  $e$  refers to the electron or positron,  $N$  is the nucleon in the initial state with momentum  $p$ , and a system  $X$  (which is not measured) is produced with momentum  $p_X$ . In case of an unpolarized nucleon, the cross-section for this process can be written in terms of the structure functions  $F_2$  and  $F_L$  in the one photon exchange approximation neglecting electroweak effects as

$$\frac{d\sigma}{dx dQ^2} = \frac{4\pi\alpha^2}{xQ^4} \left[ \left(1 - y + \frac{y^2}{2}\right) F_2(x, Q^2) - \frac{y^2}{2} F_L(x, Q^2) \right]. \quad (\text{A.2})$$

Instead of structure functions, the reduced cross-section  $\sigma_r$  is often used

$$\sigma_r = \frac{d^2\sigma}{dx dQ^2} \frac{xQ^4}{2\pi\alpha^2[1 + (1 - y)^2]} = F_2(x, Q^2) - \frac{y^2}{1 + (1 - y)^2} F_L(x, Q^2). \quad (\text{A.3})$$

With longitudinally polarized electron and nucleon beams, it is also possible to extract the structure function  $g_1$

$$\frac{1}{2} \left[ \frac{d\sigma^{\vec{\sigma}}}{dx dQ^2} - \frac{d\sigma^{\overrightarrow{\sigma}}}{dx dQ^2} \right] = \frac{4\pi\alpha^2}{Q^4} y(2 - y) g_1(x, Q^2). \quad (\text{A.4})$$

Here terms suppressed by  $x^2 m_N^2 / Q^2$  have been neglected, and  $\sigma^{\vec{\sigma}}$  refers to the case where the nucleon and electron spins are opposite (and parallel to the  $z$  axis), and  $\sigma^{\overrightarrow{\sigma}}$  to the scattering process in case of aligned spins. The kinematical variables

$x, y$  and  $Q^2$  are introduced below, and  $m_N$  is the nucleon mass and  $\alpha$  is the fine structure constant. At large  $Q^2$  and to leading order in the strong coupling constant  $\alpha_s$  the  $F_2$  structure function is proportional to the unpolarized quark and antiquark distributions in the nucleon, and  $g_1$  is sensitive to the longitudinally polarized distributions. In this limit  $F_L = 0$ , and it obtains a first contribution at next to leading order in perturbative expansion, and is thus particularly sensitive to the gluon distribution.

In diffractive (and also semi-inclusive) scattering, the process becomes

$$e(l) + N(p) \rightarrow e(l') + N'(p') + X(p_X), \quad (\text{A.5})$$

where  $N'$  refers to the nucleon or the nucleon remnants in the final state with momentum  $p'$  and a specific system  $X$  is produced. The electron mass is neglected in the following discussion, and the nucleon mass  $p^2 = m_N^2$  is kept non-zero unless otherwise stated. In this appendix,  $p$  is a four vector and  $\mathbf{p}$  and  $\mathbf{p}_\perp$  refer to the three-momentum and the transverse momentum, respectively. The momentum vectors are illustrated in Fig. A.1.

## A.2 Invariants

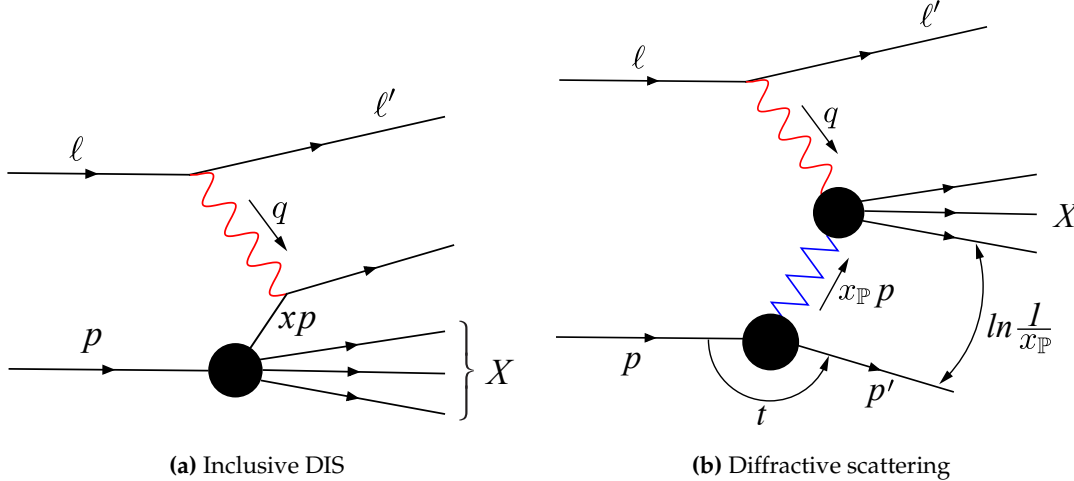


**Figure A.1:** Kinematical variables of inclusive and exclusive DIS. The blobs correspond to interactions.

Let us first consider inclusive scattering where the final state  $X$  is not completely determined and the scattered nucleon (nucleon remnants) are not reconstructed. The center-of-mass energy squared for the DIS process can be written using the momenta defined in Eq. (A.1) as

$$s = (l + p)^2 = m_N^2 + 2p \cdot l \approx 2\sqrt{E_e E_n}. \quad (\text{A.6})$$

Here  $E_e$  is the electron energy and  $E_n$  the nucleon energy, and the approximation is valid in the high energy limit where the nucleon mass can be neglected.

As the scattering process is mediated by a virtual photon, the center-of-mass energy  $W$  for the photon-nucleon system is generically more useful:

$$W^2 = (p + q)^2 = m_N^2 - Q^2 + 2p \cdot q. \quad (\text{A.7})$$

Here the virtual photon momentum is  $q = l - l'$  and its virtuality  $-Q^2 = (l - l')^2$ . The other useful Lorentz invariant quantities describing the DIS process are

$$x \equiv \frac{Q^2}{2p \cdot q} = \frac{Q^2}{2m_N \nu} = \frac{Q^2}{Q^2 + W^2 - m_N^2} \quad (\text{A.8})$$

$$y \equiv \frac{p \cdot q}{p \cdot \ell} = \frac{W^2 + Q^2 - m_N^2}{s - m_N^2} \quad (\text{A.9})$$

These invariants have intuitive physical interpretations in particular frames. The Bjorken variable  $x$  can be interpreted in the parton model in the infinite momentum frame where the nucleon carries a large longitudinal momentum. In such a frame,  $x$  is the fraction of the nucleon momentum carried by the struck parton if the quark masses are neglected. In electron-nucleon collisions,  $0 < x < 1$ .

The variable  $y$  is called *inelasticity*. When expressed in the nucleon rest frame, one finds  $y = 1 - \frac{E_l'}{E_l}$ , where  $E_l$  and  $E_l'$  are the energies of the incoming and outgoing leptons in this frame, respectively. Consequently,  $0 \leq y \leq 1$ , and in particular, the highest possible photon-nucleon center-of-mass energies are reached at the  $y \rightarrow 1$  limit. A closely related variable  $\nu$  also exists:  $\nu \equiv \frac{p \cdot q}{m_N}$  describes, in the nucleon rest frame, the electron energy carried away by the virtual photon:  $\nu = E_l - E_l'$ .

The invariants presented above are not independent, and in inclusive scattering the collision kinematics is completely determined by three variables, e.g.  $s$ ,  $Q^2$  and  $x$ . This becomes apparent when noticing that the invariants defined above satisfy e.g. the following relations:

$$Q^2 = xy(s - m_N^2), \text{ and} \quad (\text{A.10})$$

$$W^2 = \frac{1-x}{x} Q^2 + m_N^2. \quad (\text{A.11})$$

The smallest kinematically allowed virtuality  $Q_{\min}^2$  can be determined if the electron mass  $m_e$  is non-zero:  $Q_{\min}^2 = m_e^2 \frac{y^2}{1-y}$ .

Let us then discuss diffractive production of a system  $X$  with an invariant mass  $M_X^2$ . In the unpolarized case where the cross-section is symmetric in azimuthal

angle, we can describe the kinematics by introducing the following new invariants:

$$t \equiv -(p' - p)^2 \quad (\text{A.12})$$

$$x_{\mathbb{P}} \equiv \frac{(p - p') \cdot q}{p \cdot q} = \frac{M_X^2 + Q^2 - t}{W^2 + Q^2 - m_N^2} \quad (\text{A.13})$$

$$\beta \equiv \frac{Q^2}{2q \cdot (p - p')} = \frac{Q^2}{M_X^2 + Q^2 - t} \quad (\text{A.14})$$

In the infinite momentum frame,  $x_{\mathbb{P}}$  has the interpretation that in the scattering process an exchange of vacuum quantum numbers (a *pomeron* exchange) takes place, and the pomeron carries a fraction of  $x_{\mathbb{P}}$  of the nucleon longitudinal momentum. Similarly, in the partonic language  $\beta$  is the longitudinal momentum of the struck parton inside the pomeron. These invariants are not independent, and can be related to the invariants of inclusive DIS discussed above via e.g.

$$x = \beta x_{\mathbb{P}}. \quad (\text{A.15})$$

An experimental signature of a diffractive event is the presence of a rapidity gap between the outgoing nucleon (nucleon remnants) and the system X. This gap size is  $\Delta y \sim \ln 1/x_{\mathbb{P}}$ .

### A.3 Laboratory frame

In the laboratory frame the collisions are asymmetric, and the inclusive DIS invariants can be determined by measuring the energy and the scattering angle of the outgoing electron. In the limit of small nucleon mass, the invariants read

$$s = 4E_e E_n \quad (\text{A.16})$$

$$Q^2 = 2E_e E'_e (1 - \cos \theta_e) \quad (\text{A.17})$$

$$W^2 = 4E_e E_n - 2E'_e [E_n + E_e + (E_n - E_e) \cos \theta_e] \quad (\text{A.18})$$

$$x = \frac{E_e E'_e (1 - \cos \theta_e)}{2E_e E_n - E'_e E_n (1 + \cos \theta_e)} \quad (\text{A.19})$$

$$y = \frac{2E_e E_n - E'_e E_n (1 + \cos \theta_e)}{2E_e E_n}. \quad (\text{A.20})$$

Here  $E_e$  and  $E'_e$  are the incoming and outgoing electron energies, and the electron scattering angle is  $\theta_e$ , with  $\theta_e = 0$  corresponding to the forward scattering, or photoproduction region  $Q^2 \approx 0$ . Similarly the incoming nucleon energy is  $E_n$ .

In exclusive processes it is possible to also measure the momentum of the produced particle and its invariant mass by measuring the decay products. Although the kinematical variables can be reconstructed using the scattered electron only,

a common method to determine  $y$  and  $Q^2$  is to express these invariants in terms of the scattering angles of both the electron and the produced particle using the double angle method [31]:

$$Q^2 = 4E_e^2 \frac{\sin \theta_e (1 - \cos \theta_V)}{\sin \theta_V + \sin \theta_e - \sin(\theta_e + \theta_V)} \quad (\text{A.21})$$

$$y = \frac{\sin \theta_e (1 - \cos \theta_V)}{\sin \theta_V + \sin \theta_e - \sin(\theta_e + \theta_V)}. \quad (\text{A.22})$$

Here  $\theta_V$  is the scattering angle of the produced particle. These expressions are again valid in the limit where the nucleon mass can be neglected, and other similar methods can be found from Ref. [31]. Note that once  $Q^2$  and  $y$  are determined,  $x$  and  $W^2$  can be obtained using Eqs. (A.10) and (A.11).

The squared momentum transfer  $t$  can be written as

$$t = -\frac{(\mathbf{p}_{X\perp} - \mathbf{l}'_{\perp})^2 + x_{\mathbb{P}}^2 m_N^2}{1 - x_{\mathbb{P}}} \approx -(\mathbf{p}_{X\perp} - \mathbf{l}'_{\perp})^2. \quad (\text{A.23})$$

Here  $\mathbf{p}_{X\perp}$  is the transverse momentum of the produced particle and  $\mathbf{l}'_{\perp}$  the transverse momentum of the scattered electron, and the approximation is valid at high energies where  $x_{\mathbb{P}}$  is small and the momentum transfer is approximatively transverse. Note that the kinematical lower bound for  $t$  reads

$$-t > -t_{\min} = \frac{x_{\mathbb{P}}^2 m_N^2}{1 - x_{\mathbb{P}}}. \quad (\text{A.24})$$

When  $t$ ,  $Q^2$  and  $W^2$  are determined,  $x_{\mathbb{P}}$  can be obtained by using Eq. (A.13).

In exclusive and semi-inclusive processes the particle  $X$  is identified by measuring the invariant mass of the decay products. In inclusive diffraction the invariant mass  $M_X^2$  is determined by measuring the total energy  $E_X$  and the total momentum  $\mathbf{p}_X$  of the produced particles:

$$M_X^2 = E_X^2 - \mathbf{p}_X^2. \quad (\text{A.25})$$

In these events, it is also possible to construct inelasticity using the hadron method

$$y_h = \frac{E_X - \mathbf{p}_{Xz}}{2E_e}. \quad (\text{A.26})$$

The hadron method can also be used to determine inelasticity in exclusive particle production in the photoproduction limit where the scattered electron cannot be detected. For a better experimental accuracy, different methods to construct e.g. inelasticity can be combined (see e.g. [32]). Generically in inclusive diffraction  $M_X^2 + Q^2 \gg |t|$ , and consequently  $t$  can be neglected when determining  $x_{\mathbb{P}}$  and  $\beta$

using Eqs. (A.13) and (A.14).

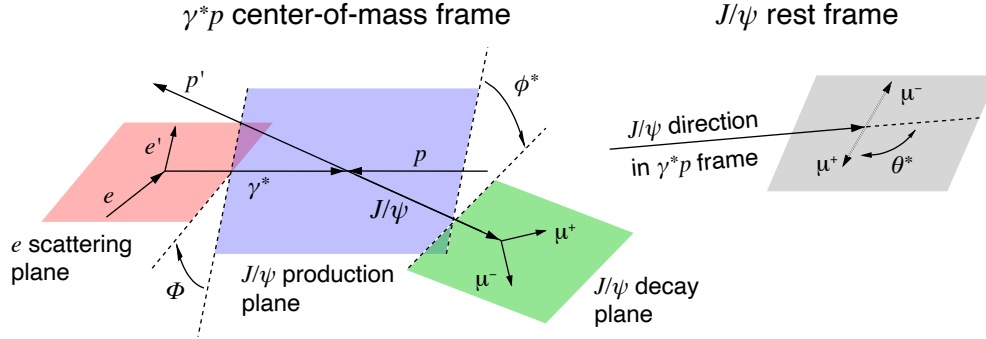


Figure A.2: Planes in exclusive vector meson production.

## A.4 Breit frame

A natural frame to describe hard scattering process in DIS is the Breit (or brick wall) frame, where the incoming photon carries no energy, and the parton to which the photon couples to behaves as if it bounced off a brick wall. Let us choose that the ultrarelativistic nucleon moves along the positive  $z$  axis, and the photon propagates to the  $-z$  direction. The nucleon momentum in this frame is  $p_z = \frac{1}{2x}Q$ , and the parton longitudinal momentum  $k_z$  can be written as  $k_z = xp_z = \frac{1}{2}Q$ . Similarly, the photon four-momentum reads  $q = (0, 0, 0, -Q)$ . Now, after the photon absorption  $\mathbf{k}' = -\mathbf{k}$ , where  $\mathbf{k}'$  is the parton momentum after the scattering. Note that in this frame there is no energy transfer to the proton.

The Breit frame is not the center-of-mass frame for the parton-photon scattering. This is advantageous when separating the produced particles from the beam remnants. In the Breit frame, the produced particles populate the region of negative  $z$  momentum, while the beam remnants generically have a positive momentum  $z$  component.

## A.5 Helicity studies

Studying the helicity structure of exclusive particle production processes requires one to measure the azimuthal angles  $\phi^*$  and  $\Phi$  defined in Fig. A.2. Note that the angles are defined in the frame where the photon and the nucleon momenta are aligned along the same axis (here  $z$  axis), so this discussion is valid both in the Breit frame and in the  $\gamma$ -nucleon center-of-mass frame.

The production plane is defined as the plane spanned by the  $z$  axis and the momentum of the produced particle. The azimuthal angle between this plane, and

the electron scattering plane spanned by the momenta of the incoming and outgoing electron momentum vectors is denoted by  $\Phi$  in Fig. A.2, where the geometry is illustrated in case of  $e^+ + p \rightarrow e^+ + p + J/\psi$  scattering. Similarly, we define the decay plane, which is spanned by the momenta of the decay products of the produced particle, and the azimuthal angle between this plane and the production plane is denoted by  $\phi^*$ .

The third angle required to specify the geometry  $\theta^*$  also shown in Fig. A.2 is required to determine the polarization state of the produced particle. This angle is defined as the polar angle of the decay particle having the same charge as the incoming lepton in the rest frame of the decaying particle. The  $\theta^* = 0$  case corresponds to the direction of the produced particle in the photon-nucleon center-of-mass frame.





# Appendix B

## Author List

R. Abdul Khalek<sup>1,2</sup>, A. Accardi<sup>3,4</sup>, J. Adam<sup>5</sup>, D. Adamiak<sup>6</sup>, W. Akers<sup>4</sup>, M. Albaladejo<sup>4</sup>, A. Al-bataineh<sup>7</sup>, M.G. Alexeev<sup>8,9</sup>, F. Ameli<sup>10</sup>, P. Antonioli<sup>11</sup>, N. Armesto<sup>12</sup>, W.R. Armstrong<sup>13</sup>, M. Arratia<sup>14,4</sup>, J. Arrington<sup>15,\$</sup>, A. Asaturyan<sup>16</sup>, M. Asai<sup>17</sup>, E.C. Aschenauer<sup>5,+</sup>, S. Aune<sup>18</sup>, H. Avagyan<sup>4</sup>, C. Ayerbe Gayoso<sup>19</sup>, B. Azmoun<sup>5</sup>, A. Bacchetta<sup>20,21</sup>, M.D. Baker<sup>5</sup>, F. Barbosa<sup>4</sup>, L. Barion<sup>4,22</sup>, K.N. Barish<sup>14,\*,\$</sup>, P.C. Barry<sup>23</sup>, M. Battaglieri<sup>4,24</sup>, A. Bazilevsky<sup>5</sup>, N.K. Behera<sup>25</sup>, F. Benmokhtar<sup>26</sup>, V.V. Berdnikov<sup>27,+</sup>, J.C. Bernauer<sup>28,29,30</sup>, V. Bertone<sup>18</sup>, S. Bhattacharya<sup>31</sup>, C. Bissolotti<sup>20,21</sup>, D. Boer<sup>32,\$</sup>, M. Boglione<sup>8,9</sup>, M. Bondi<sup>24</sup>, P. Boora<sup>33</sup>, I. Borsa<sup>34</sup>, F. Bossù<sup>18</sup>, G. Bozzi<sup>20,21</sup>, J.D. Brandenburg<sup>5,30</sup>, N. Brei<sup>4</sup>, A. Bressan<sup>35,36,+</sup>, W.K. Brooks<sup>37,+</sup>, S. Bufalino<sup>9,38</sup>, M.H.S. Bukhari<sup>39</sup>, V. Burkert<sup>4</sup>, N.H. Buttmore<sup>40</sup>, A. Camsonne<sup>4</sup>, A. Celentano<sup>24,+</sup>, F.G. Celiberto<sup>20,41,42,43</sup>, W. Chang<sup>5,44</sup>, C. Chatterjee<sup>36</sup>, K. Chen<sup>5</sup>, T. Chetry<sup>19</sup>, T. Chiarusi<sup>11</sup>, Y.-T. Chien<sup>30</sup>, M. Chiosso<sup>8,9</sup>, X. Chu<sup>5</sup>, E. Chudakov<sup>4,+</sup>, G. Cicala<sup>45,46</sup>, E. Cisebani<sup>47,10</sup>, I.C. Cloet<sup>13</sup>, C. Cocuzza<sup>31</sup>, P.L. Cole<sup>48</sup>, D. Colella<sup>45,49</sup>, J.L. Collins II<sup>50</sup>, M. Constantinou<sup>31</sup>, M. Contalbrigo<sup>22</sup>, G. Contin<sup>35,36</sup>, R. Corliss<sup>28,30</sup>, W. Cosyn<sup>51,+</sup>, A. Courtoy<sup>52</sup>, J. Crafts<sup>27</sup>, R. Cruz-Torres<sup>15</sup>, R.C. Cuevas<sup>4</sup>, U. D'Alesio<sup>53,54</sup>, S. Dalla Torre<sup>36,\*,\$</sup>, D. Das<sup>55</sup>, S.S. Dasgupta<sup>36</sup>, C. Da Silva<sup>56</sup>, W. Deconinck<sup>57,\$</sup>, M. Defurne<sup>18</sup>, W. DeGraw<sup>58</sup>, K. Dehmelt<sup>28,30</sup>, A. Del Dotto<sup>59</sup>, F. Delcarro<sup>4</sup>, A. Deshpande<sup>28,5,30</sup>, W. Detmold<sup>60</sup>, R. De Vita<sup>24</sup>, M. Diefenthaler<sup>4,\*,\$</sup>, C. Dilks<sup>61</sup>, D.U. Dixit<sup>58</sup>, S. Dulat<sup>62</sup>, A. Dumitru<sup>63,\*,\$</sup>, R. Dupré<sup>64,+</sup>, J.M. Durham<sup>56</sup>, M.G. Echevarria<sup>65</sup>, L. El Fassi<sup>19</sup>, D. Elia<sup>45,+</sup>, R. Ent<sup>4,\$</sup>, R. Esha<sup>28,30</sup>, J.J. Ethier<sup>2</sup>, O. Evdokimov<sup>66,\*,\$</sup>, K.O. Eyser<sup>5</sup>, C. Fanelli<sup>60</sup>, R. Fatemi<sup>67,+</sup>, S. Fazio<sup>5,30,+</sup>, C. Fernandez-Ramirez<sup>52</sup>, M. Finger<sup>68</sup>, M. Finger Jr.<sup>68</sup>, D. Fitzgerald<sup>69</sup>, C. Flore<sup>64</sup>, T. Frederico<sup>70</sup>, I. Frišić<sup>60,4</sup>, S. Fucini<sup>71,72</sup>, S. Furletov<sup>4</sup>, Y. Furletova<sup>4,+</sup>, C. Gal<sup>30,28</sup>, L. Gamberg<sup>73</sup>, H. Gao<sup>61</sup>, P. Garg<sup>30</sup>, D. Gaskell<sup>4,+</sup>, K. Gates<sup>74</sup>, M.B. Gay Ducati<sup>75</sup>, M. Gericke<sup>57</sup>, G. Gil Da Silveira<sup>75</sup>, F.-X. Girod<sup>76,77</sup>, D.I. Glazier<sup>74</sup>, K. Gnanvo<sup>78,+</sup>, V.P. Goncalves<sup>79</sup>, L. Gonella<sup>80</sup>, J.O. Gonzalez Hernandez<sup>8,9</sup>, Y. Goto<sup>81</sup>, F. Grancagnolo<sup>82</sup>, L.C. Greiner<sup>15,+</sup>, W. Guryn<sup>5</sup>, V. Guzey<sup>83</sup>, Y. Hatta<sup>5</sup>, M. Hattawy<sup>84</sup>, F. Hauenstein<sup>84,60</sup>, X. He<sup>85</sup>, T.K. Hemmick<sup>30,28,+</sup>, O. Hen<sup>60,+</sup>, G. Heyes<sup>4</sup>, D.W. Higinbotham<sup>4,+,#</sup>, A.N. Hiller Blin<sup>4</sup>, T.J. Hobbs<sup>4,86,87</sup>, M. Hohlmann<sup>50</sup>, T. Horn<sup>27,4,\*,\$</sup>, T.-J. Hou<sup>88</sup>, J. Huang<sup>5</sup>, Q. Huang<sup>18</sup>, G.M. Huber<sup>89</sup>, C.E. Hyde<sup>84</sup>, G. Iakovidis<sup>5</sup>, Y. Ilieva<sup>90</sup>, B.V. Jacak<sup>58,15,\$</sup>, P.M. Jacobs<sup>15</sup>, M. Jadhav<sup>13</sup>, Z. Janoska<sup>91</sup>, A. Jentsch<sup>5,+</sup>, T. Jezo<sup>92</sup>, X. Jing<sup>86</sup>, P.G. Jones<sup>80,\*,\$</sup>, K. Joo<sup>76</sup>, S. Joosten<sup>13</sup>, V. Kafka<sup>91</sup>, N. Kalantarians<sup>93</sup>, G. Kalicy<sup>27</sup>, D. Kang<sup>94</sup>, Z.B. Kang<sup>95</sup>, K. Kauder<sup>5,30</sup>, S.J.D. Kay<sup>89</sup>, C.E. Keppel<sup>4</sup>, J. Kim<sup>13</sup>, A. Kiselev<sup>5,+</sup>, M. Klasen<sup>96</sup>, S. Klein<sup>15,+</sup>, H.T. Kleist<sup>28</sup>, O. Korchak<sup>91</sup>, A. Kostina<sup>91</sup>, P. Kotko<sup>97</sup>, Y.V. Kovchegov<sup>6</sup>, M. Krelina<sup>91</sup>, S. Kuleshov<sup>98</sup>, S. Kumano<sup>99</sup>, K.S. Kumar<sup>100</sup>, R. Kumar<sup>101</sup>, L. Kumar<sup>102</sup>, K. Kumerički<sup>103</sup>, A. Kusina<sup>104</sup>, K. Kutak<sup>104</sup>, Y.S. Lai<sup>15</sup>, K. Lalwani<sup>33</sup>, T. Lappi<sup>105,106,+</sup>, J. Lauret<sup>5</sup>, M. Lavinsky<sup>50</sup>, D. Lawrence<sup>4</sup>, D. Lednicky<sup>91</sup>, C. Lee<sup>56</sup>, K. Lee<sup>15</sup>, S.H. Lee<sup>69</sup>, S. Levorato<sup>36</sup>, H. Li<sup>107</sup>, S. Li<sup>15</sup>, W. Li<sup>108</sup>, X. Li<sup>56</sup>, X. Li<sup>61</sup>, W.B. Li<sup>109,4</sup>, T. Ligonzo<sup>110,45</sup>, H. Liu<sup>100</sup>, M.X. Liu<sup>56</sup>, X. Liu<sup>111</sup>, S. Liuti<sup>78</sup>, N. Liyanage<sup>78</sup>, C. Lorcé<sup>112</sup>, Z. Lu<sup>113</sup>, G. Lucero<sup>34</sup>, N.S. Lukow<sup>31</sup>, E. Lunghi<sup>114</sup>, R. Majka<sup>115</sup>, Y. Makris<sup>21</sup>, I. Mandjavidze<sup>18</sup>, S. Mantry<sup>116</sup>, H. Mäntysaari<sup>105,106</sup>, F. Marhauser<sup>4</sup>, P. Markowitz<sup>51</sup>, L. Marsicano<sup>24</sup>, A. Mastroserio<sup>117,45</sup>, V. Mathieu<sup>118</sup>, Y. Mehtar-Tani<sup>29</sup>, W. Melnitchouk<sup>4</sup>, L. Mendez<sup>119,+</sup>, A. Metz<sup>31,\*,\$</sup>, Z.-E. Meziani<sup>13</sup>, C. Mezrag<sup>18</sup>, M. Mihovilović<sup>120</sup>, R. Milner<sup>60,\$</sup>, M. Mirazita<sup>59</sup>, H. Mkrtchyan<sup>16</sup>, A. Mkrtchyan<sup>16</sup>, V. Mochalov<sup>121,122</sup>, V. Moiseev<sup>121</sup>, M.M. Mondal<sup>30,28</sup>, A. Morreale<sup>56</sup>, D. Morrison<sup>5</sup>, L. Motyka<sup>123</sup>, H. Moutarde<sup>18</sup>, C. Muñoz Camacho<sup>64,\*,\$</sup>, F. Murgia<sup>54</sup>, M.J. Murray<sup>124,+</sup>, P. Musico<sup>24</sup>, P. Nadel-Turonski<sup>28,30</sup>, P.M. Nadolsky<sup>86</sup>, J. Nam<sup>31</sup>, P.R. Newman<sup>80,+</sup>, D. Neyret<sup>18,+</sup>, D. Nguyen<sup>4</sup>,

E.R. Nocera<sup>125</sup>, F. Noferini<sup>11</sup>, F. Noto<sup>126</sup>, A.S. Nunes<sup>5</sup>, V.A. Okorokov<sup>122</sup>, F. Olness<sup>86</sup>, J.D. Osborn<sup>119</sup>, B.S. Page<sup>5,30,+</sup>, S. Park<sup>28</sup>, A. Parker<sup>26</sup>, K. Paschke<sup>78</sup>, B. Pasquini<sup>20,21,+</sup>, H. Paukkunen<sup>105</sup>, S. Paul<sup>14</sup>, C. Pecar<sup>61</sup>, I.L. Pegg<sup>27</sup>, C. Pellegrino<sup>127</sup>, C. Peng<sup>13</sup>, L. Pentchev<sup>4</sup>, R. Perrino<sup>45</sup>, F. Petriello<sup>13,128,+</sup>, R. Petti<sup>90</sup>, A. Pilloni<sup>10</sup>, C. Pinkenburg<sup>5</sup>, B. Pire<sup>112</sup>, C. Pisano<sup>53,54</sup>, D. Pitonyak<sup>129</sup>, A.A. Poblaguev<sup>5</sup>, T. Polakovic<sup>13</sup>, M. Posik<sup>31</sup>, M. Potekhin<sup>5</sup>, R. Preghenella<sup>11</sup>, S. Preins<sup>14</sup>, A. Prokudin<sup>73,4</sup>, P. Pujahari<sup>130</sup>, M.L. Purschke<sup>5</sup>, J.R. Pybus<sup>60,4</sup>, M. Radici<sup>21,\$</sup>, R. Rajput-Ghoshal<sup>4</sup>, P.E. Reimer<sup>13</sup>, M. Rinaldi<sup>71,72</sup>, F. Ringer<sup>15</sup>, C.D. Roberts<sup>131</sup>, S. Rodini<sup>20,21</sup>, J. Rojo<sup>1,2</sup>, D. Romanov<sup>4</sup>, P. Rossi<sup>4,59,+</sup>, E. Santopinto<sup>24</sup>, M. Sarsour<sup>85</sup>, R. Sassot<sup>34</sup>, N. Sato<sup>4,+</sup>, B. Schenke<sup>5</sup>, W.B. Schmidke<sup>5</sup>, I. Schmidt<sup>37</sup>, A. Schmidt<sup>77</sup>, B. Schmookler<sup>30,28,+</sup>, G. Schnell<sup>132,133</sup>, P. Schweitzer<sup>76</sup>, J. Schwiening<sup>134</sup>, I. Scimemi<sup>118</sup>, S. Scopetta<sup>71,72</sup>, J. Segovia<sup>135</sup>, R. Seidl<sup>81,29,+</sup>, S. Sekula<sup>86</sup>, K. Semenov-Tian-Shanskiy<sup>83</sup>, D.Y. Shao<sup>94</sup>, N. Sherrill<sup>114</sup>, E. Sichtermann<sup>15,+</sup>, M. Siddikov<sup>37</sup>, A. Signori<sup>20,21,4</sup>, B.K. Singh<sup>136</sup>, S. Širca<sup>137,120</sup>, K. Slifer<sup>138</sup>, W. Slominski<sup>123</sup>, D. Sokhan<sup>74,+</sup>, W.E. Sondheim<sup>56</sup>, Y. Song<sup>58</sup>, O. Soto<sup>59</sup>, H. Spiesberger<sup>139</sup>, A.M. Stasto<sup>140,+</sup>, P. Stepanov<sup>27</sup>, G. Sterman<sup>28,30</sup>, J.R. Stevens<sup>109,+</sup>, I.W. Stewart<sup>60</sup>, I. Strakovsky<sup>77</sup>, M. Strikman<sup>140</sup>, M. Sturm<sup>61</sup>, M.L. Stutzman<sup>4</sup>, M. Sullivan<sup>17</sup>, B. Surrow<sup>31,\$</sup>, P. Svihra<sup>91</sup>, S. Syritsyn<sup>28,30</sup>, A. Szczepaniak<sup>114</sup>, P. Sznajder<sup>141</sup>, H. Szumila-Vance<sup>4</sup>, L. Szymanowski<sup>141</sup>, A.S. Tadealli<sup>4</sup>, J.D. Tapia Takaki<sup>124</sup>, G.F. Tassielli<sup>82</sup>, J. Terry<sup>95</sup>, F. Tassarotto<sup>36</sup>, K. Tezgin<sup>76</sup>, L. Tomasek<sup>91</sup>, F. Torales Acosta<sup>58</sup>, P. Tribedy<sup>5</sup>, A. Tricoli<sup>5</sup>, Triloki<sup>36</sup>, S. Tripathi<sup>142</sup>, R.L. Trotta<sup>27</sup>, O.D. Tsai<sup>95</sup>, Z. Tu<sup>5,30</sup>, C. Tuvè<sup>143,144</sup>, T. Ullrich<sup>5,30,115,\$</sup>, M. Ungaro<sup>4</sup>, G.M. Urciuoli<sup>10</sup>, A. Valentini<sup>110,45</sup>, P. Vancura<sup>91</sup>, M. Vandenbroucke<sup>18</sup>, C. Van Hulse<sup>64</sup>, G. Varner<sup>142</sup>, R. Venugopalan<sup>5,30</sup>, I. Vitev<sup>56,+</sup>, A. Vladimirov<sup>145,+</sup>, G. Volpe<sup>110,45</sup>, A. Vossen<sup>61,4,+</sup>, E. Voutier<sup>64</sup>, J. Wagner<sup>141</sup>, S. Wallon<sup>64</sup>, H. Wang<sup>4</sup>, Q. Wang<sup>124</sup>, X. Wang<sup>146</sup>, S.Y. Wei<sup>41,42</sup>, C. Weiss<sup>4</sup>, T. Wenaus<sup>5,+</sup>, H. Wennlöf<sup>80</sup>, N. Wickramaarachchi<sup>27</sup>, A. Wikramanayake<sup>50</sup>, D. Winney<sup>114</sup>, C.P. Wong<sup>56</sup>, C. Woody<sup>5</sup>, L. Xia<sup>147</sup>, B.W. Xiao<sup>148,+</sup>, J. Xie<sup>13</sup>, H. Xing<sup>107</sup>, Q.H. Xu<sup>149</sup>, J. Zhang<sup>30,149</sup>, S. Zhang<sup>4</sup>, Z. Zhang<sup>5</sup>, Z.W. Zhao<sup>61</sup>, Y.X. Zhao<sup>150</sup>, L. Zheng<sup>151</sup>, Y. Zhou<sup>109</sup>, and P. Zurita<sup>145</sup>

<sup>1</sup>Vrije Universiteit Amsterdam, 1081 HV Amsterdam, The Netherlands

<sup>2</sup>Nikhef Theory Group, 1098 XG Amsterdam, The Netherlands

<sup>3</sup>Hampton University, Hampton, Virginia 23668, USA

<sup>4</sup>Thomas Jefferson National Accelerator Facility, Newport News, Virginia 23606, USA

<sup>5</sup>Brookhaven National Laboratory, Upton, New York 11973, USA

<sup>6</sup>Ohio State University, Columbus, Ohio 43210, USA

<sup>7</sup>Imam Abdulrahman Bin Faisal Univ., Dammam 34212, Saudi Arabia

<sup>8</sup>Università di Torino, I-10125 Torino, Italy

<sup>9</sup>INFN - Sezione di Torino, I-10125 Torino, Italy

<sup>10</sup>INFN - Sezione di Roma, I-00185 Roma, Italy

<sup>11</sup>INFN - Sezione di Bologna, I-40127 Bologna, Italy

<sup>12</sup>Universidad de Santiago de Compostela, E-15705 Santiago de Compostela, Spain

<sup>13</sup>Argonne National Laboratory, Lemont, Illinois 60439, USA

<sup>14</sup>University of California at Riverside, Riverside, California 92521, USA

<sup>15</sup>Lawrence Berkeley National Laboratory, Berkeley, California 94720, USA

<sup>16</sup>A. Alikhanian National Science Laboratory, Armenia

<sup>17</sup>SLAC National Accelerator Laboratory, Menlo Park, California 94025, USA

<sup>18</sup>IRFU, CEA, Université Paris-Saclay, F-91191 Gif-sur-Yvette, France

<sup>19</sup>Mississippi State University, Starkville, Mississippi 39762, USA

<sup>20</sup>Università di Pavia, I-27100 Pavia, Italy

<sup>21</sup>INFN - Sezione di Pavia, I-27100 Pavia, Italy

<sup>22</sup>INFN - Sezione di Ferrara, I-44122 Ferrara, Italy

<sup>23</sup>North Carolina State University, Raleigh, North Carolina 27607, USA

<sup>24</sup>INFN - Sezione di Genova, I-16146 Genova, Italy

<sup>25</sup>Central University of Tamil Nadu, Tamil Nadu 610005, India

<sup>26</sup>Duquesne University, Pittsburgh, Pennsylvania 15282, USA

<sup>27</sup>The Catholic University of America, Washington, DC 20064, USA

<sup>28</sup>Stony Brook University, Stony Brook, New York 11794, USA

<sup>29</sup>RIKEN BNL Research Center - Brookhaven National Laboratory, Upton, New York 11973, USA

<sup>30</sup>CFNS, Stony Brook, New York 11794, USA

<sup>31</sup>Temple University, Philadelphia, Pennsylvania 19122, USA

<sup>32</sup>University of Groningen, 9712 CP Groningen, The Netherlands

<sup>33</sup>MNIT Jaipur, Jaipur, Rajasthan 302017, India

<sup>34</sup>Universidad de Buenos Aires, C1053 CABA, Argentina

<sup>35</sup>Università di Trieste, I-34127 Trieste, Italy

<sup>36</sup>INFN - Sezione di Trieste, I-34149 Trieste, Italy

<sup>37</sup>Universidad Técnica Federico Santa María, Valparaíso, Chile

- <sup>38</sup> Politecnico di Torino, I-10129 Torino, Italy
- <sup>39</sup> Jazan University, Jazan, Saudi Arabia
- <sup>40</sup> Trinity College, Dublin 2, Ireland
- <sup>41</sup> ECT\*, I-38123 Villazzano (Trento), Italy
- <sup>42</sup> Fondazione Bruno Kessler (FBK), I-38123 Povo (Trento), Italy
- <sup>43</sup> INFN - TIFPA, I-38123 Povo (Trento), Italy
- <sup>44</sup> Central China Normal University, Wuhan, Hubei 430079, China
- <sup>45</sup> INFN - Sezione di Bari, I-70126 Bari, Italy
- <sup>46</sup> CNR-ISTP Bari, I-70126 Bari, Italy
- <sup>47</sup> Istituto Superiore di Sanità, I-00161 Roma, Italy
- <sup>48</sup> Lamar University, Beaumont, Texas 77705, USA
- <sup>49</sup> Politecnico di Bari, I-70126 Bari, Italy
- <sup>50</sup> Florida Institute of Technology, Melbourne, Florida 32901, USA
- <sup>51</sup> Florida International University, Miami, Florida 33199, USA
- <sup>52</sup> Universidad Nacional Autónoma de México, 36 01000 Ciudad de México, Mexico
- <sup>53</sup> Università di Cagliari, I-09042 Monserrato (Cagliari), Italy
- <sup>54</sup> INFN - Sezione di Cagliari, I-09042 Monserrato (Cagliari), Italy
- <sup>55</sup> Saha Institute of Nuclear Physics, Kolkata, West Bengal 700064, India
- <sup>56</sup> Los Alamos National Laboratory, Los Alamos, New Mexico 87545, USA
- <sup>57</sup> University of Manitoba, Winnipeg, Manitoba R3T 2N2, Canada
- <sup>58</sup> University of California Berkeley, Berkeley, California 94720, USA
- <sup>59</sup> INFN - LNF, I-00044 Frascati (Roma), Italy
- <sup>60</sup> Massachusetts Institute of Technology, Cambridge, Massachusetts 02139, USA
- <sup>61</sup> Duke University, Durham, North Carolina 27708, USA
- <sup>62</sup> Xinjiang University, Urumqi, Xinjiang 830046, China
- <sup>63</sup> Baruch College - The City University of New York, New York City, New York 10010, USA
- <sup>64</sup> Université Paris-Saclay, CNRS - IJCLab, F-91406 Orsay, France
- <sup>65</sup> Universidad de Alcalá, 28805 Alcalá de Henares, Madrid, Spain
- <sup>66</sup> University of Illinois at Chicago, Chicago, Illinois 60607, USA
- <sup>67</sup> University of Kentucky, Lexington, Kentucky 40506, USA
- <sup>68</sup> Charles University, 116 36 Prague 1, Czech Republic
- <sup>69</sup> University of Michigan, Ann Arbor, Michigan 48109, USA
- <sup>70</sup> Instituto Tecnológico de Aeronáutica, 12.228-900 São José dos Campos, Brazil
- <sup>71</sup> Università di Perugia, I-06123 Perugia, Italy
- <sup>72</sup> INFN - Sezione di Perugia, I-06123 Perugia, Italy
- <sup>73</sup> Penn State Univ.-Berks, Reading, Pennsylvania 19610, USA
- <sup>74</sup> University of Glasgow, Glasgow G12 8QQ, Scotland, United Kingdom
- <sup>75</sup> Universidade Federal do Rio Grande do Sul, 91501-970 Porto Alegre, RS, Brazil
- <sup>76</sup> University of Connecticut, Storrs, Connecticut 06269, USA
- <sup>77</sup> The George Washington University, Washington, DC 20052, USA
- <sup>78</sup> University of Virginia, Charlottesville, Virginia 22904, USA
- <sup>79</sup> Universidade Federal de Pelotas, CEP 96010-900 Pelotas, RS, Brazil
- <sup>80</sup> University of Birmingham, Birmingham B15 2TT, United Kingdom
- <sup>81</sup> RIKEN Nishina Center for Accelerator-Based Science, Wako, Saitama 351-0198, Japan
- <sup>82</sup> INFN - Sezione di Lecce, I-73100 Lecce, Italy
- <sup>83</sup> Petersburg Nuclear Physics Institute, Gatchina 188300, Russia
- <sup>84</sup> Old Dominion University, Norfolk, Virginia 23529, USA
- <sup>85</sup> Georgia State University, Atlanta, Georgia 30302, USA
- <sup>86</sup> Southern Methodist University, Dallas, Texas 75275, USA
- <sup>87</sup> Illinois Institute of Technology, Chicago, Illinois 60616, USA
- <sup>88</sup> Northeastern University, Shenyang, Liaoning, China
- <sup>89</sup> University of Regina, Regina, Saskatchewan S4S 0A2, Canada
- <sup>90</sup> University of South Carolina, Columbia, South Carolina 29208, USA
- <sup>91</sup> Czech Technical University, 115 19 Prague 1, Czech Republic
- <sup>92</sup> Karlsruhe Institute of Technology, 76128 Karlsruhe, Germany
- <sup>93</sup> Virginia Union University, Richmond, Virginia 23220, USA
- <sup>94</sup> Fudan University, Shanghai 200433, China
- <sup>95</sup> University of California at Los Angeles, Los Angeles, California 90095, USA
- <sup>96</sup> Westfälische Wilhelms-Universität Münster, 48149 Münster, Germany
- <sup>97</sup> AGH University of Science and Technology, 30-059 Krakow, Poland
- <sup>98</sup> Universidad Andres Bello, Sazié 2212, Piso 7, Santiago, Chile
- <sup>99</sup> KEK, Tsukuba, Ibaraki 305-0801, Japan
- <sup>100</sup> University of Massachusetts, Amherst, Massachusetts 01003, USA
- <sup>101</sup> Akal University, Talwandi Sabo, Punjab 151302, India

- <sup>102</sup> *Panjab University, Chandigarh 160014, India*
- <sup>103</sup> *University of Zagreb, 10000 Zagreb, Croatia*
- <sup>104</sup> *Institute of Nuclear Physics Polish Academy of Sciences, PL-31342 Krakow, Poland*
- <sup>105</sup> *University of Jyväskylä, 40014 Jyväskylä, Finland*
- <sup>106</sup> *Helsinki Institute of Physics, FI-00014 Helsinki, Finland*
- <sup>107</sup> *South China Normal University, Guangzhou 510631, China*
- <sup>108</sup> *Rice University, Houston, Texas 77005, USA*
- <sup>109</sup> *The College of William and Mary, Williamsburg, Virginia 23185, USA*
- <sup>110</sup> *Università di Bari, I-70121 Bari, Italy*
- <sup>111</sup> *Beijing Normal University, Beijing 100875, China*
- <sup>112</sup> *CNRS - CPHT, École Polytechnique, I.P. Paris, F-91120 Palaiseau, France*
- <sup>113</sup> *Southeast University, Nanjing, Jiangsu 211189, China*
- <sup>114</sup> *Indiana University, Bloomington, Indiana 47405, USA*
- <sup>115</sup> *Yale University, New Haven, Connecticut 06520, USA*
- <sup>116</sup> *University of North Georgia, Dahlonega, Georgia 30597, USA*
- <sup>117</sup> *Università di Foggia, I-71122 Foggia, Italy*
- <sup>118</sup> *Universidad Complutense de Madrid, E-28040 Madrid, Spain*
- <sup>119</sup> *Oak Ridge National Laboratory, Oak Ridge, Tennessee 37830, USA*
- <sup>120</sup> *Jožef Stefan Institute, 1000 Ljubljana, Slovenia*
- <sup>121</sup> *NRC "Kurchatov Institute" - IHEP, Protvino, Moscow region 142280, Russia*
- <sup>122</sup> *National Research Nuclear University MEPhI, Moscow 115409, Russia*
- <sup>123</sup> *Jagiellonian University, PL-31007 Krakow, Poland*
- <sup>124</sup> *University of Kansas, Lawrence, Kansas 66045, USA*
- <sup>125</sup> *University of Edinburgh, JCMB, KB, Edinburgh EH9 3FD United Kingdom*
- <sup>126</sup> *INFN - LNS, I-95123 Catania, Italy*
- <sup>127</sup> *INFN - CNAF, I-40127 Bologna, Italy*
- <sup>128</sup> *Northwestern University, Evanston, Illinois 60208, USA*
- <sup>129</sup> *Lebanon Valley College, Annville, Pennsylvania 17003, USA*
- <sup>130</sup> *IIT Madras, Chennai, Tamil Nadu 600036, India*
- <sup>131</sup> *Nanjing University, Nanjing, Jiangsu 210093, China*
- <sup>132</sup> *University of the Basque Country UPV/EHU, E-48940 Bilbao, Spain*
- <sup>133</sup> *IKERBASQUE, Basque Foundation for Science, E-48009 Bilbao, Spain*
- <sup>134</sup> *GSI Helmholtzzentrum für Schwerionenforschung GmbH, Darmstadt, Germany*
- <sup>135</sup> *Universidad Pablo de Olavide, E-41013 Sevilla, Spain*
- <sup>136</sup> *Banaras Hindu University, Varanasi, Uttar Pradesh 221005, India*
- <sup>137</sup> *University of Ljubljana, 1000 Ljubljana, Slovenia*
- <sup>138</sup> *University of New Hampshire, Durham, New Hampshire 03824, USA*
- <sup>139</sup> *Johannes Gutenberg Universität, D-55122 Mainz, Germany*
- <sup>140</sup> *The Pennsylvania State University, University Park, Pennsylvania 16802, USA*
- <sup>141</sup> *National Centre for Nuclear Research (NCBJ), 02-093 Warsaw, Poland*
- <sup>142</sup> *University of Hawaii, Honolulu, Hawaii 96822, USA*
- <sup>143</sup> *Università di Catania, I-95124 Catania, Italy*
- <sup>144</sup> *INFN - Sezione di Catania, I-95125 Catania, Italy*
- <sup>145</sup> *Universitaet Regensburg, D-93040 Regensburg, Germany*
- <sup>146</sup> *Zhengzhou University, Zhengzhou, Henan 450001, China*
- <sup>147</sup> *University of Science and Technology of China, Hefei, Anhui 230052, China*
- <sup>148</sup> *The Chinese University of Hong Kong, Hong Kong, Shenzhen 518172, China*
- <sup>149</sup> *Shandong University, Qingdao, Shandong 266237, China*
- <sup>150</sup> *Chinese Academy of Sciences, Lanzhou, Gansu Province 730000, China*
- <sup>151</sup> *China University of Geosciences, Wuhan, Hubei 430079, China*

\$ Editor

\* Working Group Convener

+ Sub-Working Group Convener

# Technical Editor

# Appendix C

## Organizational Structure

### Physics working group and sub-working group conveners

- Physics Working Group conveners: Adrian Dumitru (The City University of New York, USA), Olga Evdokimov (University of Illinois Chicago, USA), Andreas Metz (Temple University, USA), and Carlos Muñoz Camacho (CNRS Université Paris-Saclay, France)
- Inclusive Reactions:  
Conveners: Renee Fatemi (University of Kentucky, USA), Nobuo Sato (JLab, USA), Barak Schmookler (Stony Brook University, USA)
- Semi-inclusive Reactions:  
Conveners: Ralf Seidl (RIKEN, Japan), Justin Stevens (The College of William&Mary, USA), Alexey Vladimirov (University of Regensburg, Germany), Anselm Vossen (Duke University, USA), Bowen Xiao (The China University of Hong Kong, China)
- Jets, Heavy Quarks:  
Conveners: Leticia Mendez (ORNL, USA), Brian Page (BNL, USA), Frank Petriello (ANL & Northwestern University, USA), Ernst Sichtermann (LBNL, USA), Ivan Vitev (LANL, USA)
- Exclusive Reactions:  
Conveners: Raphaël Dupré (CNRS Université Paris-Saclay, France), Salvatore Fazio (BNL, USA), Tuomas Lappi (University of Jyväskylä, Finland), Barbara Pasquini (University of Pavia, Italy), Daria Sokhan (University of Glasgow, Scotland-UK)
- Diffractive Reactions & Tagging:  
Conveners: Wim Cosyn (Florida International University, USA), Or Hen (MIT, USA), Douglas Higginbotham (JLab, USA), Spencer Klein (LBNL, USA), Anna Stasto (Penn State University, USA)

### Detector working group and sub-working group conveners

- Detector Working Group conveners: Ken Barish (UC Riverside, USA), Silvia Dalla Torre (INFN - Trieste, Italy), Tanja Horn (The Catholic University of America, USA), Peter Jones (University of Birmingham, UK), and Markus Diefenthaler, ex-officio (JLab, USA)

- Tracking (+vertexing)  
Conveners: Domenico Elia (INFN - Bari, Italy), Kondo Gnanvo (University of Virginia, USA), Leo Greiner (LBNL, USA)
- Particle ID  
Conveners: Tom Hemmick (Stony Brook University, USA), Patrizia Rossi (JLab, USA)
- Calorimetry (EM and Hadronic)  
Conveners: Vladimir Berdnikov (The Catholic University of America, USA), Eugene Chudakov (JLab, USA)
- Far-Forward Detectors  
Conveners: Alexander Jentsch (BNL, USA), Michael Murray (University of Kansas, USA)
- DAQ/Electronics  
Conveners: Andrea Celentano (INFN - Genova, Italy), Damien Neyret (CEA Saclay, France)
- Polarimetry/ Ancillary Detectors  
Conveners: Elke Aschenauer (BNL, USA), Dave Gaskell (JLab, USA)
- Central Detector/Integration & Magnet  
Conveners: William Brooks (University of Valparaiso, Chile), Alexander Kiselev (BNL, USA)
- Forward Detector/IR Integration  
Convener: Yulia Furletova (JLab, USA)
- Detector Complementarity  
Conveners: Elke Aschenauer (BNL, USA), Paul Newman (University of Birmingham, UK)

### **Software working group conveners**

- Andrea Bressan (INFN - Trieste, Italy), Markus Diefenthaler (JLab, USA), Torre Wenaus (BNL, USA)

### **EIC User Group Steering Committee**

- Chair: Bernd Surrow (Temple University, USA), Vice-Chair: Richard Milner (MIT, USA)
- At Large Members: John Arrington (ANL, USA), Marco Radici (INFN - Pavia, Italy), Barbara Jacak (LBNL and UC Berkeley, USA)
- Lab Representatives: Thomas Ullrich (BNL, USA), Rolf Ent (JLab, USA)
- European Representative: Daniel Boer (University Groningen, NL)
- International Representative: Wouter Deconinck (University of Manitoba, CA)
- Institutional Board Chair (ex-officio): Christine Aidala (University of Michigan, USA)

# Appendix D

## Acknowledgements

The EIC yellow report was the result of a year long community wide effort. The authors are indebted to the following colleagues for critical and crucial comments in the preparation of this report: Iris Abt (MPI-Munich, Germany), Ani Aprahamyan (AANL, Armenia), Barbara Badelek (Univ. Warsaw, Poland), Marie Boer (Virginia Tech., USA), Helen Caines (Yale Univ., USA), Maria Chamizo-Llatas (BNL, USA), Janusz Chwastowski (IFJ PAN, Poland), Dmitry Denisov (BNL, USA), Markus Diehl (DESY, Germany), Haiyan Gao (Duke Univ., USA), Michel Garçon (IRFU CEA-Saclay, France), Donald Geesaman (ANL, USA), Ed Kinney (Univ. Colorado-Boulder, USA), Robert Klanner (Univ. Hamburg, Germany), Christina Markert (Univ. Texas at Austin, USA), Bob McKeown (JLab, USA), Hugh Montgomery (JLab, USA), Piet Mulders (Vrije Univ. and NIKHEF, Amsterdam, the Netherlands), Eugenio Nappi (INFN-Bari, Italy), Peter Petreczky (BNL, USA), Krzysztof Piotrkowski (Cath. Univ. Louvain, Belgium), Oscar Rondon-Aramayo (Univ. Virginia, USA), James Symons (LBNL, USA), Cristina Tuvè (Univ. and INFN - Catania, Italy), Julia Velkovskaja (Vanderbilt Univ., USA), and Glenn Young (BNL, USA). The EICUG Steering Committee is also indebted to Rik Yoshida for conceptualizing the Yellow Report Initiative in the early stages

We acknowledge support from the following institutions/agencies:

1. DOE, Office of Science, Office of Nuclear Physics (USA)

**Contracts:** DE-AC05-06OR23177, DE-AC02-05CH11231, DE-AC02-06CH11357, DE-AC52-06NA25396, DE-FG02-87ER40365, DE-FG02-88ER40410, DE-FG02-93ER40771, DE-FG02-94ER40818, DE-FG02-03ER41260, DE-FG02-04ER41325, DE-FG02-07ER41460, DE-FG02-09ER41620, DE-SC0004286, DE-SC0008791, DE-SC0010129, DE-SC0020240, DE-SC0020265, DE-SC0012704, DE-SC0016583, DE-SC0020405, DE-SC0011090, DE-SC0013391, DE-SC0018224, DE-SC0019230, DE-SC001012, DE-SC0013405

2. European Union

**Projects:** CA 1521

**ERC:** ERC-2018-ADG-835105, ERC-2015-CoG-681707

**Horizon 2020 programme:**

**Contracts:** STRONG-2020 n. 824093, AIDA-2020 n. 654168

**MSCA:** "RISE" n. 823947, "ParDHonSFF" n. 752748, "SQuHadron" n. 795475, "FELLINI" n. 754496

3. National Science Foundation (USA)

**Awards:** n. 2012826, 2000108, 1812423

**Grants:** n. PHY-1915093, PHY-1714133, PHY-2012430, PHY-2012002, PHY-1945471, DGE-1650604

4. Brookhaven National Laboratory (USA)

**Programs:** LDRD n. 18-037

5. the Netherlands Organization for Scientific Research (NWO - the Netherlands)

6. German Research Foundation (DFG - Germany)

**Grants:** KL 1266/9-1, 396021762-TRR257, FOR 2926

7. National Science Center (NCN - Poland)

**Grants:** n. 2017/26/M/ST2/01074, 2017/27/B/ST2/02755, 2019/33/B/ST2/02588,  
2019/34/E/ST2/00186, 2019/35/D/ST2/00272

8. National Council of Science and Technology (CONICET - Argentina)

9. Academy of Finland

**Projects:** n. 308301, 314764, 321840

10. Italian Ministry of Education, University and Research (MIUR - Italy)

**"FARE" grants:** "3DGLUE" n. R16XKPHL3N

11. Spanish Ministry of Science and Innovation (MICINN - Spain)

**Grants:** n. FPA2017-83814-P, MDM-2016-0692, PID2019-107844GB-C22, PID2019-106080GB-C21

12. Xunta de Galicia (Spain)

**Projects:** ED431C 2017/07, ED431G 2019/05

13. Junta de Andalucía (Spain)

**Contracts:** n. P18-FRJ-1132

**Programs:** "Operativo FEDER 2014-2020" n. UHU-1264517

14. Research Talent Attraction Program (Comunidad Autónoma de Madrid - Spain)

**Contracts:** n. 2018-T1/TIC-10313

15. Natural Sciences and Engineering Research Council of Canada (NSERC - Canada)

**Contracts:** n. SAPIN-2016-00031

16. Los Alamos National Laboratory (USA)

**Programs:** LDRD n. 20200022DR

17. Science and Technology Facilities Council (STFC - United Kingdom)

**Grants:** n. ST/T000600/1

18. National Agency of Research and Development (ANID - Chile)

**Grants:** FONDECYT n. 1191103, 1180232, PIA/APOYO AFB 180002

19. National Autonomous University of Mexico (UNAM - Mexico)

**Grants:** DGAPA-PAPIIT n. IA 1017120, IN 106921

20. National Council of Science and Technology (CONACyT - Mexico)

**Grants:** "Ciencia de Frontera 2019" n. 51244 (FORDECYT-PRONACES), n. A1-S-21389

21. Czech Ministry of Education, Youth and Sport (MEYS - Czech Republic)



- Grants:** n. LM2015054, LM2018109
22. Chinese University of Hong Kong (CUHK Shenzhen - China)  
**Grants:** n. UDF01001859
23. Guangdong Major Project of Basic and Applied Basic Research (Guangdong - China)  
**Projects:** n. 2020B0301030008
24. National Natural Science Foundation of China (NSFC - China)  
**Grants:** n. 11875112, 11775023, 12022512
25. Hundred Talents Plan for Professionals (Jiangsu Province - China)
26. Simons Foundation (New York City - USA)  
**Grants:** "Investigator" n. 327942
27. National Council of Scientific and Technological Involvement (CNPq - Brazil)  
**Grants:** n. 308486/2015-3
28. The São Paulo Research Foundation (FAPESP - Brazil)  
**Grants:** n. 17/05660-0
29. National Institute of Science and Technology - Nuclear Physics and Applications (INCT-FNA - Brazil)  
**Grants:** n. 464898/2014-5
30. Argonne National Laboratory (USA)  
**Programs:** LDRD
31. Lawrence Berkeley National Laboratory (USA)  
**Programs:** LDRD
32. University of California - Office of the President
33. Nuclear Science and Security Consortium (California - USA)
34. Slovenian Research Agency (ARRS - Slovenia)

A.B, M.D., and T. W. thank EIC-India for their help with benchmarks and validation of the simulation software, V.V.B. thanks Tanja Horn for the support, T.J.H. acknowledges partial support from the JLab EIC Center, and S.H.L. thanks Christine Aidala for the support and critical revision of his work.



# References

- [1] National Academies of Sciences, Engineering, and Medicine, An Assessment of U.S.-Based Electron-Ion Collider Science, The National Academies Press, Washington, DC, 2018. doi:10.17226/25171.
- [2] A. Accardi, et al., Electron Ion Collider: The Next QCD Frontier: Understanding the glue that binds us all, Eur. Phys. J. A 52 (2016) 268. arXiv:1212.1701, doi:10.1140/epja/i2016-16268-9.
- [3] A. Aprahamian, et al., Reaching for the horizon: The 2015 long range plan for nuclear science, DOE/NSF Nuclear Science Advisory Panel Report (2015). URL <http://www.osti.gov/biblio/1296778>
- [4] R. L. Jaffe, A. Manohar, The G(1) problem: fact and fantasy on the spin of the proton, Nucl. Phys. B 337 (1990) 509–546. doi:10.1016/0550-3213(90)90506-9.
- [5] E.-C. Aschenauer, et al., The RHIC SPIN Program: Achievements and Future Opportunities (2015). arXiv:1501.01220.
- [6] E. C. Aschenauer, R. Sassot, M. Stratmann, Unveiling the proton spin decomposition at a future Electron-Ion Collider, Phys. Rev. D 92 (2015) 094030. arXiv:1509.06489, doi:10.1103/PhysRevD.92.094030.
- [7] E. C. Aschenauer, S. Fazio, J. H. Lee, H. Mantysaari, B. S. Page, B. Schenke, T. Ullrich, R. Venugopalan, P. Zurita, The Electron-Ion Collider: Assessing the energy dependence of key measurements, Rept. Prog. Phys. 82 (2019) 024301. arXiv:1708.01527, doi:10.1088/1361-6633/aaf216.
- [8] X.-D. Ji, A QCD analysis of the mass structure of the nucleon, Phys. Rev. Lett. 74 (1995) 1071–1074. arXiv:hep-ph/9410274, doi:10.1103/PhysRevLett.74.1071.
- [9] C. Lorcé, On the hadron mass decomposition, Eur. Phys. J. C 78 (2) (2018) 120. arXiv:1706.05853, doi:10.1140/epjc/s10052-018-5561-2.
- [10] Y. Hatta, A. Rajan, K. Tanaka, Quark and gluon contributions to the QCD trace anomaly, JHEP 12 (2018) 008. arXiv:1810.05116, doi:10.1007/JHEP12(2018)008.

- [11] A. Metz, B. Pasquini, S. Rodini, Revisiting the proton mass decomposition, *Phys. Rev. D* 102 (11) (2021) 114042. [arXiv:2006.11171](#), [doi:10.1103/PhysRevD.102.114042](#).
- [12] A. C. Aguilar, et al., Pion and Kaon Structure at the Electron-Ion Collider, *Eur. Phys. J. A* 55 (10) (2019) 190. [arXiv:1907.08218](#), [doi:10.1140/epja/i2019-12885-0](#).
- [13] D. Boer, P. J. Mulders, Time reversal odd distribution functions in lepto-production, *Phys. Rev. D* 57 (1998) 5780–5786. [arXiv:hep-ph/9711485](#), [doi:10.1103/PhysRevD.57.5780](#).
- [14] D. W. Sivers, Single Spin Production Asymmetries from the Hard Scattering of Point-Like Constituents, *Phys. Rev. D* 41 (1990) 83. [doi:10.1103/PhysRevD.41.83](#).
- [15] D. W. Sivers, Hard scattering scaling laws for single spin production asymmetries, *Phys. Rev. D* 43 (1991) 261–263. [doi:10.1103/PhysRevD.43.261](#).
- [16] L. Zheng, E. C. Aschenauer, J. H. Lee, B.-W. Xiao, Z.-B. Yin, Accessing the gluon Sivers function at a future electron-ion collider, *Phys. Rev. D* 98 (3) (2018) 034011. [arXiv:1805.05290](#), [doi:10.1103/PhysRevD.98.034011](#).
- [17] D. Müller, D. Robaschik, B. Geyer, F. M. Dittes, J. Hořejši, Wave functions, evolution equations and evolution kernels from light ray operators of QCD, *Fortsch. Phys.* 42 (1994) 101–141. [arXiv:hep-ph/9812448](#), [doi:10.1002/prop.2190420202](#).
- [18] A. V. Radyushkin, Scaling limit of deeply virtual Compton scattering, *Phys. Lett. B* 380 (1996) 417–425. [arXiv:hep-ph/9604317](#), [doi:10.1016/0370-2693\(96\)00528-X](#).
- [19] X.-D. Ji, Deeply virtual Compton scattering, *Phys. Rev. D* 55 (1997) 7114–7125. [arXiv:hep-ph/9609381](#), [doi:10.1103/PhysRevD.55.7114](#).
- [20] M. Burkardt, Impact parameter space interpretation for generalized parton distributions, *Int. J. Mod. Phys. A* 18 (2003) 173–208. [arXiv:hep-ph/0207047](#), [doi:10.1142/S0217751X03012370](#).
- [21] X.-D. Ji, Gauge invariant decomposition of nucleon spin, *Phys. Rev. Lett.* 78 (1997) 610–613. [arXiv:hep-ph/9603249](#), [doi:10.1103/PhysRevLett.78.610](#).
- [22] M. Polyakov, Generalized parton distributions and strong forces inside nucleons and nuclei, *Phys. Lett. B* 555 (2003) 57–62. [arXiv:hep-ph/0210165](#), [doi:10.1016/S0370-2693\(03\)00036-4](#).
- [23] E.-C. Aschenauer, S. Fazio, K. Kumericki, D. Mueller, Deeply Virtual Compton Scattering at a Proposed High-Luminosity Electron-Ion Collider, *JHEP* 09 (2013) 093. [arXiv:1304.0077](#), [doi:10.1007/JHEP09\(2013\)093](#).

- [24] F. Gelis, E. Iancu, J. Jalilian-Marian, R. Venugopalan, The Color Glass Condensate, *Ann. Rev. Nucl. Part. Sci.* 60 (2010) 463–489. arXiv:1002.0333, doi:10.1146/annurev.nucl.010909.083629.
- [25] K. J. Eskola, P. Paakkinen, H. Paukkunen, C. A. Salgado, EPPS16: Nuclear parton distributions with LHC data, *Eur. Phys. J. C* 77 (2017) 163. arXiv:1612.05741, doi:10.1140/epjc/s10052-017-4725-9.
- [26] E. C. Aschenauer, S. Fazio, M. A. C. Lamont, H. Paukkunen, P. Zurita, Nuclear Structure Functions at a Future Electron-Ion Collider, *Phys. Rev. D* 96 (11) (2017) 114005. arXiv:1708.05654, doi:10.1103/PhysRevD.96.114005.
- [27] X. Chu, E.-C. Aschenauer, J.-H. Lee, L. Zheng, Photon structure studied at an Electron Ion Collider, *Phys. Rev. D* 96 (7) (2017) 074035. arXiv:1705.08831, doi:10.1103/PhysRevD.96.074035.
- [28] M. Arratia, Y. Song, F. Ringer, B. Jacak, Jets as precision probes in electron-nucleus collisions at the Electron-Ion Collider, *Phys. Rev. C* 101 (6) (2020) 065204. arXiv:1912.05931, doi:10.1103/PhysRevC.101.065204.
- [29] X. Liu, F. Ringer, W. Vogelsang, F. Yuan, Lepton-jet Correlations in Deep Inelastic Scattering at the Electron-Ion Collider, *Phys. Rev. Lett.* 122 (19) (2019) 192003. arXiv:1812.08077, doi:10.1103/PhysRevLett.122.192003.
- [30] J. Blumlein, The Theory of Deeply Inelastic Scattering, *Prog. Part. Nucl. Phys.* 69 (2013) 28–84. arXiv:1208.6087, doi:10.1016/j.pnpnp.2012.09.006.
- [31] S. Bentvelsen, J. Engelen, P. Kooijman, Reconstruction of  $(x, Q^2)$  and extraction of structure functions in neutral current scattering at HERA, in: *Workshop on Physics at HERA, 1992*, pp. 23–42, [https://inis.iaea.org/collection/NCLCollectionStore/\\_Public/24/039/24039755.pdf](https://inis.iaea.org/collection/NCLCollectionStore/_Public/24/039/24039755.pdf).
- [32] C. Adloff, et al., Inclusive measurement of diffractive deep inelastic ep scattering, *Z. Phys. C* 76 (1997) 613–629. arXiv:hep-ex/9708016, doi:10.1007/s002880050584.





